LANDSAT ANALYSIS FOR URANIUM EXPLORATION IN NORTHEASTERN TURKEY

by

Keenan Lee

U.S. Geological Survey, Denver, Colorado 80225

Colorado School of Mines, Golden, Colorado 80401

Open File Report 83-99

1983

LANDSAT ANALYSIS FOR URANIUM EXPLORATION IN NORTHEAST TURKEY

Keenan Lee

U.S. Geological Survey, Denver, CO

Colorado School of Mines, Golden, CO

ABSTRACT

No uranium deposits are known in the Trabzon, Turkey region, and consequently, exploration criteria have not been defined. Nonetheless, by analogy with uranium deposits studied elsewhere, exploration guides are suggested to include dense concentrations of linear features, lineaments -- especially with northwest trend, acidic plutonic rocks, and alteration indicated by limonite.

A suite of digitally processed images of a single Landsat scene served as the image base for mapping 3,376 linear features. Analysis of the linear feature data yielded two statistically significant trends, which in turn defined two sets of strong lineaments. Color composite images were used to map acidic plutonic rocks and areas of surficial limonitic materials.

The Landsat interpretation yielded a map of these exploration guides that may be used to evaluate relative uranium potential. One area in particular shows a high coincidence of favorable indicators.

INTRODUCTION

This study of Landsat images was undertaken as part of a cooperative effort between the U.S. Geological Survey and the Mineral Research and Exploration Institute of Turkey (MTA). The Trabzon area of northeastern Turkey was selected by Mssrs. Sedat Uz and Ibrahim Cetinturk of MTA as an area with uranium potential. The utility of Landsat analyses in uranium explo-

ration has been demonstrated by Raines and others (1978), Offield, Miller, and others (in press), Knepper (in press), and Raines (in press).

The purpose of this study is to provide early input to a program of regional exploration for uranium. Objectives are to provide a linear features map, a lineament map, and a geologic interpretation that would be useful in future uranium exploration.

The Trabzon study area, outlined on figure 1, includes about 70 percent of a full Landsat frame (Path 186 Row 32). The area is the central one-third of an area of interest to MTA (S. Uz and I. Cetinturk, written commun., 1980). The area is along the southeast coast of the Black Sea, about 100 km from the U.S.S.R. Elevations range from sea level to slightly above 3,000 m. Relief is high in the north, where slopes of the east-west Pontic Mountains rise steeply from the Black Sea to about 3,000 m (fig. 2). South of the Pontic Mountains divide, relief is moderate on the Anatolian Plateau, with major drainages like the Harsit and Coruh rivers flowing west and east. The southern part of the area is drained by the Euphrates River. Vegetation appears dense in the Pontic Mountains and sparse to the south.

The geology of the Trabzon area is quite complex, mostly because of Tertiary convergent-plate tectonism that has strongly deformed large areas and juxtaposed lithologies of diverse origins (Sengor and others, 1980). Brinkmann (1976) provided a summary of the geology of Turkey, and a brief description of the Trabzon 2^{o} x 3^{o} geologic map (1:500,000) was provided by Gattinger and others (1962).

The oldest sedimentary rocks are Permo-Carboniferous flysch deposits and Permian shelf facies. Paleozoic metamorphic rocks, including mica schists, quartzites, metagraywackes, quartz phyllites, graphite schists, and marbles, may be the metamorphic equivalents of these same rocks (fig. 3). Thick

sequences of Mesozoic and Tertiary shelf and trough sediments were deposited from Jurassic (Lias) time through late Miocene, while ophiolites were accumulating in the Tethys Sea to the south.

Two major periods of plutonism occurred, a late Paleozoic (Variscan) phase of granite intrusions and Tertiary (Alpidic) emplacement of granites, granodiorites, quartz monzonites, and syenites. Gattinger and others (1962, p. 41) reported that metamorphic rocks were observed "in the uppermost zones of the granites" between Gumusane and Kelkit (a region referred to in this report as the Yasdar-Kose Mountains, see fig. 2 for locations).

On a global scale, northeastern Turkey is at the convergent margin of the African (Arabian) and Eurasian plates, and as such, has experienced general north-south compression, including subduction during the closing of the Tethys Sea. On a more local scale, the North Anatolian Fault, which crosses the southern part of the study area (fig. 1), is a dextral strike-slip fault that represents a transform boundary between the smaller Turkish and Black Sea plates.

No uranium deposits have been reported in the study area, but preliminary studies by MTA (S. Uz and I. Cetinturk, written commun., 1980) show the older acidic plutonic rocks to be relatively rich in uranium, up to 18 ppm, whereas the Tertiary plutons are barren. Radioactive anomalies were found in the older acidic plutonic rocks and in overlying volcanics and fluvial sediments. A northwest system of faults contains "acidic fillings with light colors" that show wallrock alteration, sulfide mineralization, and rarely, pitchblende (S. Uz and I. Cetinturk, written commun., 1980).

Because the area of interest outlined by MTA crosses three Landsat scenes, the center scene was chosen for initial processing and analysis. The purpose of digital processing was to provide the images for interpretation of

geologic features that might indicate areas of relatively greater potential for uranium deposits. These features (discussed later) are dense concentrations of linear features, northwest lineaments, Paleozoic acidic plutonic rocks, and surficial limonite. A color infrared (CIR) image and a color-ratio composite (CRC) image were produced to aid in lithologic discrimination, in the hope of separating older from younger acidic plutonic rocks. The CRC image also was used to generate a limonite map useful for detecting areas of sulfide alteration. A Band 5/Band 6 ratio image was processed to be used in seeking anomalous vegetation patterns. Enhanced black and white images were used in addition to the above images to perform a lineament analysis that would determine those areas most favorable structurally for uranium occurrence.

Digital processing of Landsat multispectral scanner scene 20211-07214 (21 August 1975, fig. 4) provided the images used for analysis. Processing included concatenation, skewing, destriping, contrast stretching, edge enhancement, band ratioing and color compositing (described by Offield, Knepper, and others, in press). Products generated at the U.S. Geological Survey's Image Processing Laboratory include: black and white single band images with two different contrast stretches (2 percent bilinear stretch about the median and a gaussian cumulative distribution function (CDF) stretch), box filter edge-enhanced band images, color infrared composites (Bands 4, 5, 7), color coded Band 5/Band 6 ratio images, and color ratio composites (4/5, 4/6, 6/7). Offield, Knepper, and others (in press) describe these procedures used rather routinely; Siegal and Gillespie (1980, p. 209-214) should be consulted for detailed information.

LIMONITE MAPPING

The color-ratio-composite (CRC) image was generated using the following ratios: Band 4/Band 5 (0.5-0.6 μm/0.6-0.7 μm), Band 4/Band 6 (0.5-0.6 μm/0.7-0.8 μm), and Band 6/Band 7 (0.7-0.8 μm/0.8-1.1 μm). The 4/5 ratio values were coded red, the 4/6 ratio blue, and the 6/7 ratio green. In such a coding scheme, limonitic areas will image green because ferric ion absorption (crystal field transitions) near 0.9 μm causes the 6/7 ratio to be high, and the intense ferric ion absorption centered in the near ultraviolet (intervalence charge transfer between ferric and oxygen ions) causes the 4/5 and 4/6 ratios to be low. From the CRC, green areas were mapped as surfaces with limonite coatings (goethite and/or hematite).

Figure 5 is a map of limonitic areas derived from the CRC, which shows two contrasting areas - a northern area with almost no limonite and a southern area with abundant limonite. The cause of the difference is, almost surely, vegetation; the northern area corresponds to the north slope of the Pontic Mountains, where thick forests obscure the ground surface. The Anatolian region to the south appears relatively free of vegetation, but even here the mountainous regions, like the Yasdar and Kose mountains between Gumusane and Kelkit (fig. 2), show thick vegetation that precludes mapping of limonitic surfaces.

In addition to the vegetation constraint, the utility of the map is reduced further by apparent limonitic coatings on alluvial surfaces. As an exploration aid, therefore, the limonite map is severely limited.

LINEAMENT ANALYSIS

Linear Feature Mapping

Linear features (LF) were mapped by visual inspection of all of the digitally processed Landsat images and from a drainage map derived from EROS standard product images that provided sidelap and different-date stereo models. The approach was to map all linear elements or features that were recognized in the images, regardless of their source or nature, excluding only those linear features known to represent roads, canals, etc. (Sawatzky and others, 1975).

An overlay of linear features was compiled from interpretation of each of the four black/white CDF-stretched bands - that is, a single composite LF map was made that included all LFs seen sequentially on the four images. This overlay was then combined with other similar composite overlays to produce a master compilation (called "All LFs" in later illustrations). Thus seven different LF compilations were used: (1) CDF-stretched band images, (2) linear-stretched band images, (3) edge-enhanced band images, (4) 5/6 color-sliced images, (5) color IR composites (edge-enhanced and not), (6) color-ratio-composites, and (7) drainage map.

The master compilation represents, then, all LFs mapped on all images, with redundancies (it is hoped) eliminated. This compilation, shown as figure 6, includes 3,376 linear features, and it doubtless represents over-sampling of the area.

One of the original research goals of this project was to determine if significant differences exist between LF populations interpreted from different types of images (and, incidentally, from mapping by different geologists) and to try to determine if there is a "best" image. These data subsets have not yet been analyzed.

Statistical analysis of the linear feature map required digitization of the LF endpoints and subsequent data conversions using interactive computer programs (Knepper, 1975; Sawatzky and Raines, 1977, 1981). Briefly, the linear feature endpoints are converted to longitude/latitude coordinates, and LF lengths and azimuths are calculated. These data are then available for plotting programs that produce maps of the LFs and LF concentrations and for various statistical analysis routines.

Spatial Distribution of Linear Features

Figure 6 shows all linear features compiled from all of the Landsat images interpreted. This map and those that follow are UTM projections at approximately 1:1,500,000 scale.

Figure 7 maps the concentrations of all LFs of the Trabzon study area. Contour values are relative numbers that represent the number of LFs per unit area; in this example the unit cell is 4 km square. Clearly, the LFs are not uniformly distributed.

Length Distribution of Linear Features

Figure 8 is a histogram of the total LF population showing frequency of occurrence by length, in kilometers. The 3,376 LFs range from about 800 m to 17.4 km, with a mean length of 3.69 km and a median length of 3.73 km. A cumulative frequency distribution is shown in figure 9. Although a log conversion of the data was not done, the lengths are doubtless lognormally distributed (Podwysocki, 1974; written commun., 1982).

From a comparison of figures 10 and 11, showing respectively the shortest 7 percent of the LFs and the longest 5 percent, it appears to me that the shortest LFs are more uniformly (randomly?) distributed, whereas the longest LFs show more clearly preferred directions and concentrations.

Azimuth Distribution of Linear Features

A strike-frequency histogram (fig. 12) shows the frequency of occurrence of all LFs. Pixel-edge directions are N. 10° E. and N. 80° W. (280 degrees), and the sun azimuth is S. 53° E. (307 degrees).

Linear Feature Interpretation

Significant Trends

Using a significance value (defined by Sawatzky and Raines, 1981) of 90 percent, statistically significant trends are defined at five different azimuths, as shown in figure 13. There appear three main trends, a WNW trend, a narrow NNE trend, and a broad ENE trend. To determine if the two WNW trends are distinct, maps of these two subsets were compared, but finding no visual distinction between the two, they were combined into a single significant trend: Trend 1, defined as N. 78°-87° W. (273-282). A similar procedure carried out with the two ENE trends resulted also in combining these two into a single significant trend: Trend 2, defined as N. 51°-89° E. (51-89).

The LFs that trend N. 9°-11° E. are considered not to constitute a significant trend, for the following reasons:

(1) The LFs show little systematic spatial distribution (fig. 14); in particular, they do not form a strong trend parallel to their strike (fig. 15).

(2) The LFs in this azimuth are distinctly shorter than average (fig. 9),

and

(3) this is the orbital path direction, and as such, it is the direction of the pixel edges. This may be simply coincidence, but during LF mapping I believed that I was seeing edge effects and tried not to map them. Also, this trend appears on the strike-frequency histogram (fig. 12) as two lows flanking

an anomalously high, narrow trend interval. Further work on data subsets, especially comparing edge-enhanced with non-edge-enhanced images, may help clarify this question.

Because it was unknown that the 90 percent significance value used to define significant trends was necessarily the proper value, an attempt was made to interpret trends with significance values less than 90 percent. Exclusive of the three significant trends just discussed, the azimuth group with the next highest frequency of occurrence is N. 75°-76° W. (284-285). Because this subset shows little information (fig. 16), the search for significant trends ended.

Trend 1

The characteristics of the NW Trend 1 are described by:

Figure 9 - cumulative frequency distribution of lengths,

Figure 17 - spatial distribution, and

Figure 18 - concentrations of LFs.

Trend 2

The characteristics of the NE Trend 2 are described by:

Figure 9 - cumulative frequency distribution of lengths,

Figure 19 - spatial distribution, and

Figure 20 - concentrations of LFs.

Because Trend 2 is so broad, smaller subsets can be examined in 10-degree increments, as shown in figures 21-24.

Discussion

Although there are variations in detail, two prominent trends of LFs appear, a WNW trend and a broad ENE trend, with a marked paucity of LFs in between. A brief summary description of LFs at all azimuths follows:

N. 70°-90° W.: This interval contains a trend that is apparent in all data subsets.

N. 40°-70° W.: No significant trends occur. A few long linear features occur in the south of the area. A broad minimum centers about N. 51° W.; the sun azimuth is N. 53° W. Linear features in this azimuth region may be seen less clearly, and subsequently mapped at lower frequencies, because of the sun (discussed below).

N. 0°-40° W.: There may be a significant set of long LFs on the north slope of the Pontic Mountains. When a subset of LFs from this area alone was examined, a N. 15°-22° W. interval was defined using a 90 percent significance value. Similarly, a subset of LFs greater than 10 km long shows significant intervals at N. 15°-16° W. and N. 20°-22° W. (subset data are not included in this report).

N. 0°-15° E.: A well-defined, narrow trend N. 9°-11° E. appears in the central part of the image. None of these LFs is long, and there appears to be little pattern to their distribution. These LFs probably are due to pixel-edge effects.

N. 15°-50° E.: No pervasive trends occur.

N. 50°-90° E.: This interval contains the strongest of the two significant trends; the trend appears in all data subsets of all lengths and in all areas. This trend probably represents the younger set of fractures, based on the logic that Variscan fractures would occur only in Paleozoic rocks (probably less than 20 percent of image

area), except for those later reactivated, whereas younger Alpide fractures would occur in Paleozoic, Mesozoic, and lower Tertiary rocks.

An argument might be made for combining the ENE trends with the WNW trends, to form a single, 50°-wide trend. Such a trend might possibly incorporate a continuum of linear features, representing an arcuate pattern of fractures.

Because all linear feature data were derived from a single Landsat scene, it is difficult to separate out the effects of the system from the natural linear feature distribution. An attempt to do this was made in rejecting the N. 9°-11° E. trend of LFs, the pixel edge direction, but it is likely that the second pixel edge effect (N. 79°-80° W., the scanline direction) is operable as well, although these LFs could not be readily isolated in the data set.

Logic and observations elsewhere (Sawatzky and Lee, 1974) would suggest that linear features are selectively enhanced by the imaging "systems" as a function of viewing-illumination azimuths. This system effect would selectively subdue linear features in the solar illumination direction (N. 53° W.) and selectively enhance linear features oriented northeast (Briceño and Lee, in press; Briceño and others, 1982). The extent of this selective effect in this study is unknown.

Lineaments

As used in this report, a lineament is an elongate zone of small alined linear features. Except for some lineaments that appear clearly in the image itself, the recognition of lineaments is based on linear feature analysis and is the final interpretation of this analysis. The basis of lineament recognition is interpreting those linear trends, or clusters, that occur within the mapped linear features. By way of illustration, a homogeneous area

with a single fracture direction would show LFs distributed uniformly over the image, and one statistically significant trend would emerge in the analysis, but no lineament would be mapped. Thus in interpreting lineaments by the methodology used here, one normally selects a significant azimuth trend, analyzes only that subset of LFs oriented within that azimuth interval by contouring their density distribution, and selects any alined concentrations of LFs.

Figure 25 shows the lineaments that were interpreted from the northern part of the study area. With the exception of the Harsit lineament, all northwest lineaments are based on the distribution of northwest LFs (Trend 1), and all northeast lineaments similarly are derived from plots of northeast (Trend 2) LFs. Geologic rationale would suggest such lineaments to be representations of deep-seated fault zones or shear zones, along which recurring motions or adjustments take place, manifest at the surface by parallel linear topographic features, usually linear topographic lows, such as valleys and drainage segments.

The Harsit lineament is an exception to the above in that it is a northwest lineament, but it is defined on the basis of northeast linear features. The clearly defined linear concentration (fig. 20) has a trend of N. 62° W. (298). By examining subsets of the Trend 2 LFs (figs. 21-24), it becomes apparent that, although some LFs of all northeast orientations exist, the lineament is most clearly defined by the subset N. 81°-89° E. (81-89) (fig. 24).

A geologic explanation for this fracture geometry is not apparent. A possible model for the Harsit lineament might be found in an example of simple shear, with the shear couple oriented northwest and acting in a right lateral sense, with induced en echelon fractures in the shear zone approximately east-

west (analogous to fracture cleavage). Given the orientation of the Harsit lineament as N. 62° W. and an average N. 85° E. for the linear features, the average angle of intersection is 33°. The right lateral shear accords well with known current and recent tectonism if the Harsit lineament is similar to the parallel Erzincan lineament to the south (fig. 25). The Erzincan lineament is a representation of the North Anatolian Fault, the active right-lateral strike-slip fault zone (see fig. 1).

EXPLORATION GUIDES

Other studies relating Landsat features to uranium occurrences have shown a definite correlation between density of linear features and uranium deposits (Raines and others, 1978; Offield, Miller, and others, in press; Knepper, in press; Raines, in press). It may be that dense LFs correspond to numerous fractures that provide both leaching paths in the acidic source rocks and mobilization pathways along which transport and deposition of uranium take place. Using this exploration criterion, figure 7 defines three main areas of dense LF concentrations. Using the 90 contour (relative scale) to define the areas of densest concentrations of LFs, these areas were transposed to figure 26, where they are seen to lie along the Kop lineament, along the Coruh lineament, and in the Yasdar-Kose Mountains. Relatively fewer LFs were mapped in the Pontic Mountains, and they are more dispersed.

Preliminary uranium exploration conducted by MTA has suggested that northwest fractures will be more favorable than northeast fractures. This would focus attention on the northwest lineaments shown on figure 26. The northeast lineaments cannot be discounted, however, because "An alpine revival of acidic intrusive activity in the (Yasdar-Kose Mountains) region is indicated by small veins of porphyritic granites, pegmatites, and aplites" (Gattinger and others, 1962). If a later remobilization of the uranium took

place during Alpidic tectonism, deposits may then be related to the more modern stress field.

The distribution of acidic igneous rocks cannot be interpreted with any certainty. The distribution of Paleozoic acidic plutonic rocks mapped from Landsat and shown on figure 26, corresponds in general with the 1:500,000 geologic map (Gattinger and others, 1962), but there may be many more areas of similar rocks that cannot be recognized because of the vegetation in the Pontic Mountains. Acidic volcanic rocks have not been mapped. Although in some cases Eocene volcanics can be mapped on the Landsat composites, acidic rocks cannot be distinguished from intermediate and basic volcanics.

Limonitic alteration might be associated with uranium vein mineralization if pyritization occurred during mineralization. Some of the limonitic areas mapped from the CRC image (fig. 5) are shown in figure 26, but only those that correspond to bedrock (many of the limonitic areas mapped are in recent alluvial deposits). Almost no limonite could be seen in the Pontic Mountains, probably because of vegetation.

Paleozoic metamorphic rocks are not mapped, but they may provide one of the exploration criteria for allogenic deposits. Where graphite schists are common (Gattinger and others, 1962), especially around the older granites of the Yasdar-Kose Mountains, they may have provided reductants for uraniferous fluids.

Exploration guides for vein-type uranium deposits may include dense concentrations of linear features, older northwest fractures, presence of acidic rocks, especially Paleozoic granites and syenites and younger acidic volcanic rocks, limonitic alteration, and possibly older metamorphic rocks. Figure 26 is a summary compilation, derived from information shown in previous figures, of these exploration features.

SUMMARY

Landsat data have been digitally enhanced to provide images from which geologic information was extracted. Geologic interpretation has yielded guides that may be used in the regional exploration for uranium.

From enhanced images of one Landsat scene, several thousand linear features were mapped, with a median length of 3.7 km. Statistical analysis of the linear feature data defined two significant azimuth trends - a west-northwest trend (N. 78°-87° W.) and a broad northeast trend (N. 51°-89° E.). By generating contour maps of the relative concentrations of the linear features in each of these two trend intervals, derivative lineaments, usually of the same orientations, were defined. Nine strong lineaments occur, with thirteen smaller or weaker lineaments. Some pairs of west-northwest and east-northeast lineaments seem to merge, and they may, in fact, represent one long, continuous, arcuate lineament (for example, the Harsit-Coruh lineaments, see fig. 26). Known uranium deposits elsewhere correlate with dense accumulations of linear features and with lineaments.

Color infrared composites, a color-coded Band 5/Band 6 image that enhances vegetation density, and a color-ratio-composite image were used to map granitic areas south of the Pontic Mountains. These granites have an anomalously high uranium content and may be source rocks.

Limonite distribution also was mapped, in nonvegetated areas south of the Pontic Mountains, by using the color-ratio-composite image, but the results are marginal. Uranium concentrations may be associated with sulfide mineralization and alteration, and may therefore show surface limonite derived from pyrite.

A composite map of exploration guides was derived (fig. 26) from the mapping of the above geologic features on the Landsat images. Inspection of

this map may be helpful in future uranium exploration, because several areas of interest emerge. Notably, the Yasdar-Kose Mountains show a high coincidence of favorable indicators.

Because the nature of uranium deposits, if any, has not been established, the exploration criteria suggested here remain to be tested by exploration in these areas. Optimum use of these exploration guides will come with field checking, detailed field mapping, and the eventual ability to determine which of the guides is (are) the most effective.

REFERENCES CITED

Briceño, H. O., and Lee, Keenan, in press, Applications of Landsat data to geologic mapping in tropical jungle environment - Caroni River Basin, Venezuela: Proc. 16th Intl. Symp. Remote Sensing of Environment, Buenos Aires.

Briceño, H. O., Lee, Keenan, and Knepper, D. H., Jr., 1982, Analisis de lineamientos en ambiente de selva tropical, a partir de imagenes de Landsat y SLAR - cuenca media del Rio Caroni, Venezuela (Analysis of lineaments derived from Landsat and SLAR images in a tropical jungle environment - middle Caroni River Basin, Venezuela) (abs.): 1st Venezuelan Geophys. Cong., Proc., Caracas, 1982, Venez. Assoc. Geophys., p. 60-61.

Brinkmann, Roland, 1976, Geology of Turkey: Elsavier Sci. Publ. Co., Amsterdam, 158 p.

Gattinger, T. E., comp., Erentoz, Cahit, and Ketin, Ihsan, eds., 1962, Turkiye jeoloji haritasi 1:500,000 olcekli-Trabzon (Geologic map of Turkey, 1:500,000 scale - Trabzon [Quadrangle]): Maden Tetkik ve Arama Enstitusu, Ankara, 75 p.

Knepper, D. H., Jr., ed., 1975, Geologic and mineral and water resources investigations in western Colorado, using ERTS-1 data: Final Report, NASA Contract NAS 5-21778: Colo. School of Mines, Remote Sensing Rept. 75-1, p. 95-135.

_____ in press, Sandstone uranium deposits and Landsat linear features in the southern Colorado Plateau - some observations: Symp. uranium exploration methods, Paris, 1982, Organization for Economic Cooperation and Development.

Offield, T. W., Knepper, D. H., Jr., Sawatzky, D. L., and Raines, G. L., in press, Regional settings of uranium occurrence: Preliminary Landsat studies - Introduction: Symp. uranium exploration methods, Paris, 1982, Organization for Economic Cooperation and Development.

Offield, T. W., Miller, G. B., Raines, G. L., and Ramaekers, Paul, in press, Unconformity-vein uranium setting in Saskatchewan, Canada - preliminary Landsat study: Symp. uranium exploration methods, Paris, 1982, Organization for Economic Cooperation and Development.

Podwysocki, M. H., 1974, An analysis of fracture trace patterns in areas of flat-lying sedimentary rocks for the detection of buried geologic structure: Goddard Space Flight Center, Greenbelt, Md., (X-923-74-200) 67 p.

Raines, G. L., in press, Regional analysis of Landsat data concerning unconformity-vein uranium deposits, Pine Creek Geosyncline, Australia: Symp. uranium exploration methods, Paris, 1982, Organization for Economic Cooperation and Development.

Raines, G. L., Offield, T. W., and Santos, E. S., 1978, Remote sensing and subsurface definition of facies and structure related to uranium deposits, Powder River Basin, Wyoming: Econ. Geology, v. 73, no. 1, p. 1706.

Sawatzky, D. L., and Lee, Keenan, 1974, New uses of shadow enhancement: Remote Sensing of Earth Resources, v. 3, p. 1-18.

Sawatzky, D. L., Prost, G. L., Lee, Keenan, and Knepper, D. H., Jr., 1975, Geological significance of features observed in Colorado from orbital altitudes: Proc. First Earth Resources Survey Symp., NASA, Houston, v. 1B, p. 713-760.

Sawatzky, D. L., and Raines, G. L., 1977, Analysis of lineament trends and intersections (abs.): Geol. Soc. America Abstracts with Programs, v. 9, no. 6, p. 759.

_____ 1981, Geologic uses of linear feature maps from small-scale images, in O'Leary, D. W., and Earl, J. L., eds., 3rd Intl. Conf. New Basement Tectonics, Proc.: Denver, Basement Tectonics Comm., p. 91-100.

Sengor, A. M. C., Yilmaz, Yucel, and Ketin, Ihsan, 1980, Remnants of pre-Late Jurassic ocean in northern Turkey: fragments of Permian-Triassic Paleo-Tethys?: Geol. Soc. America Bull., Pt. I, v. 91, p. 599-609.

Siegal, B. S., and Gillespie, A. R., 1980, Remote sensing in geology: John Wiley and Sons, New York, 702 p.

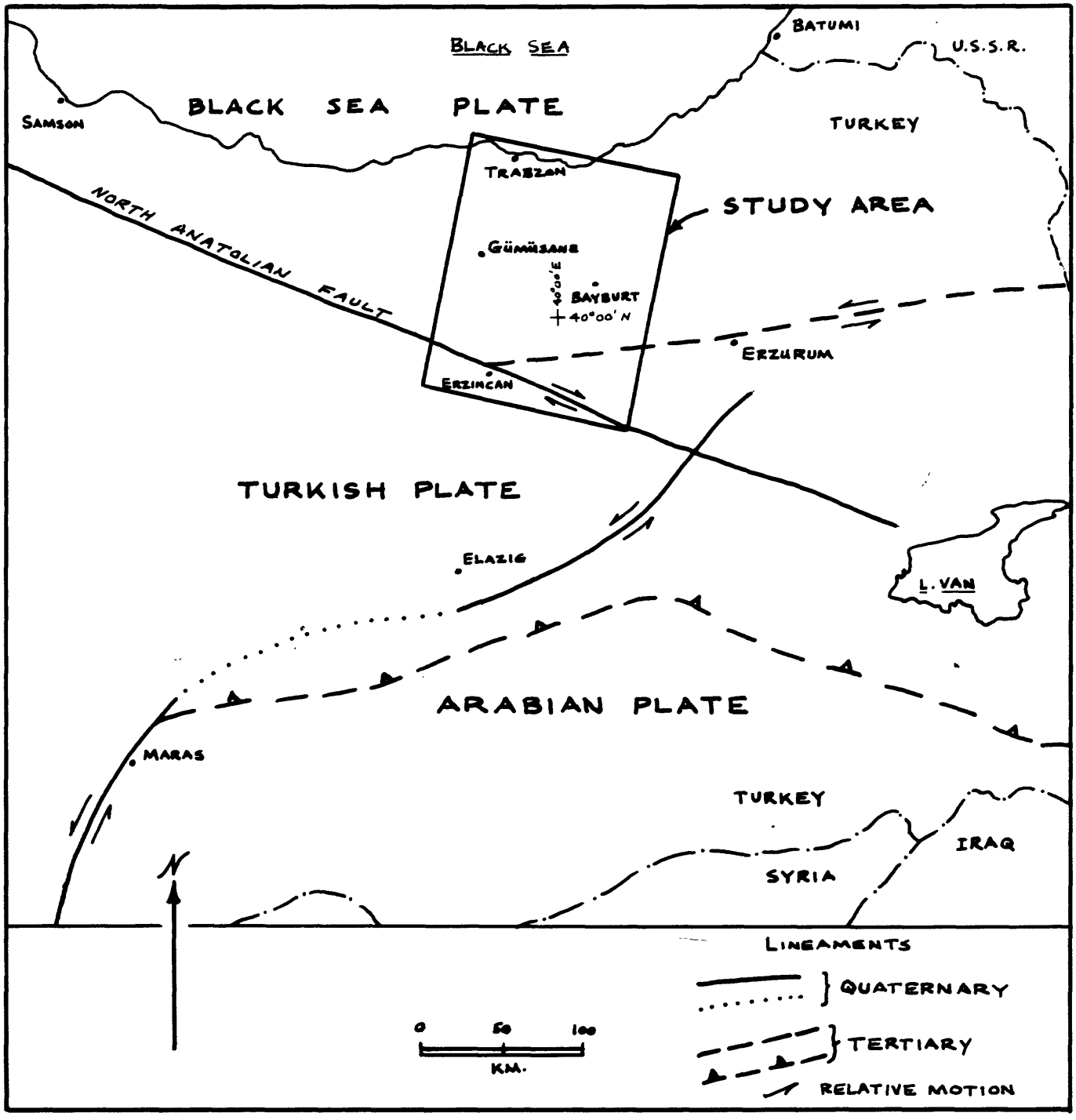

Figure 1. Location of study area with respect to regional tectonic elements (from Brinkmann, 1976).

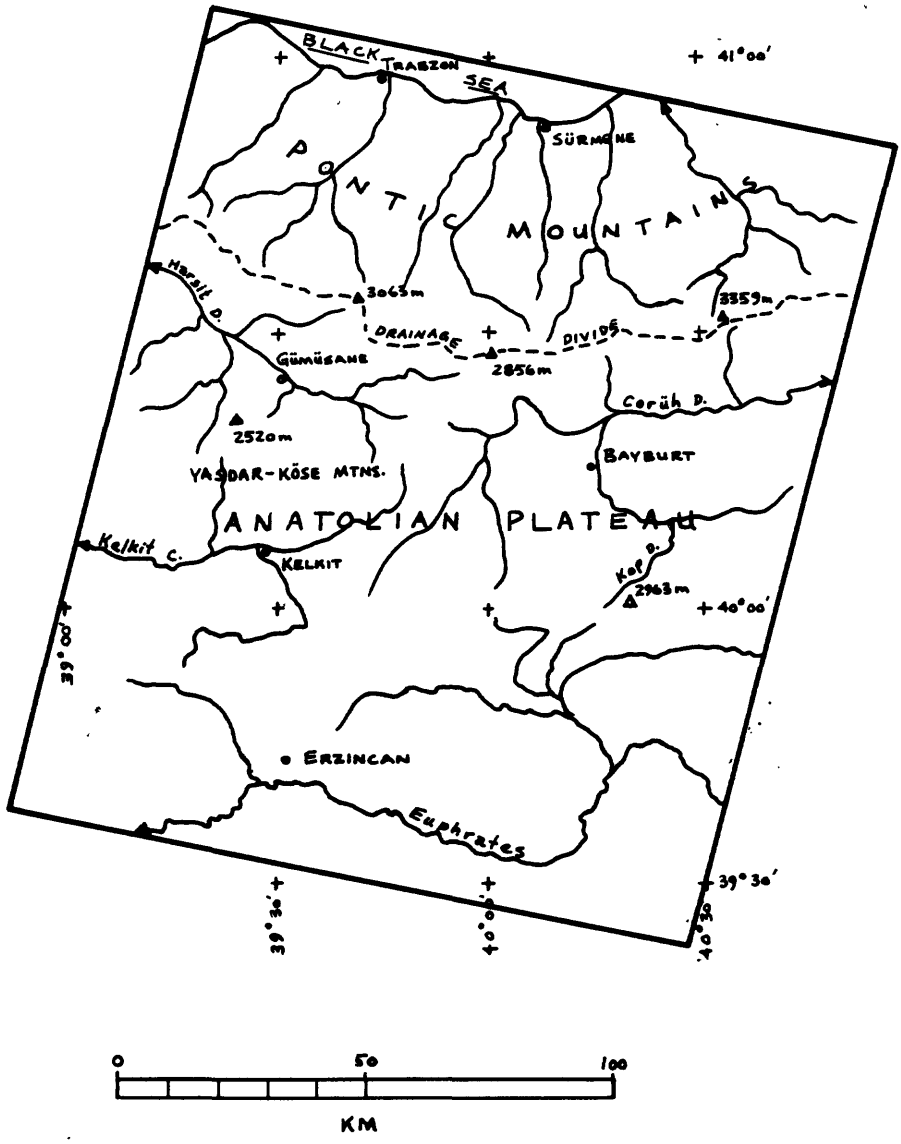

Figure 2. Index map of study area.

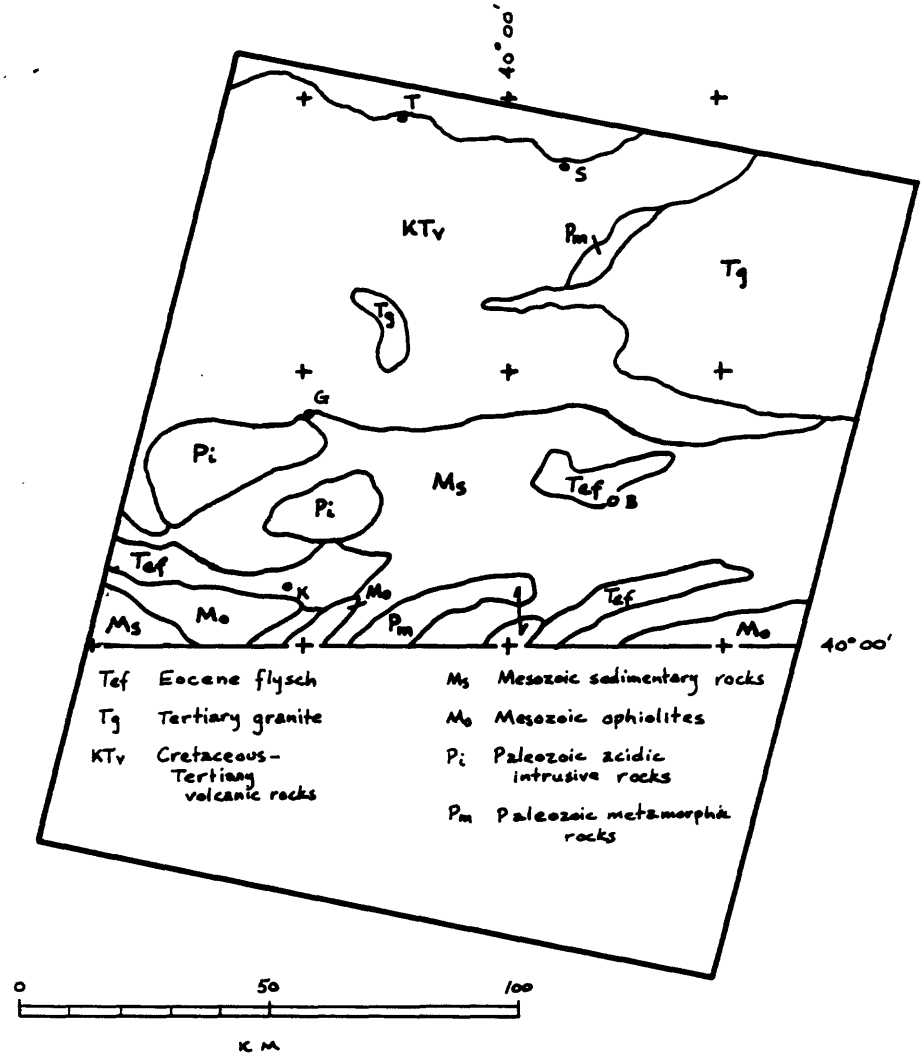

Figure 3. Geologic sketch map of northern part of study area (simplified from Gattinger and others, 1962).

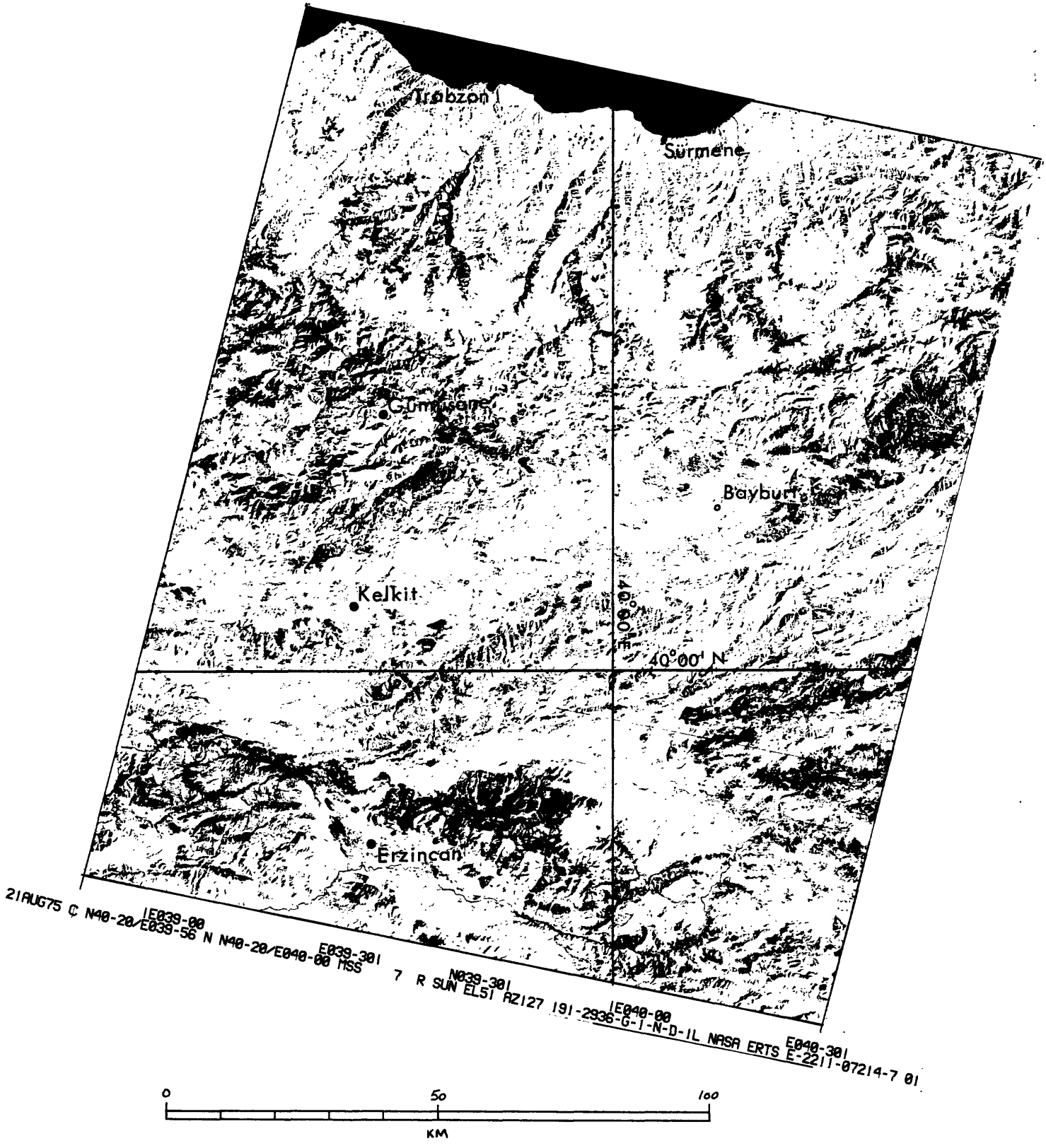

Figure 4. Landsat image of Trabzon study area (not enhanced).

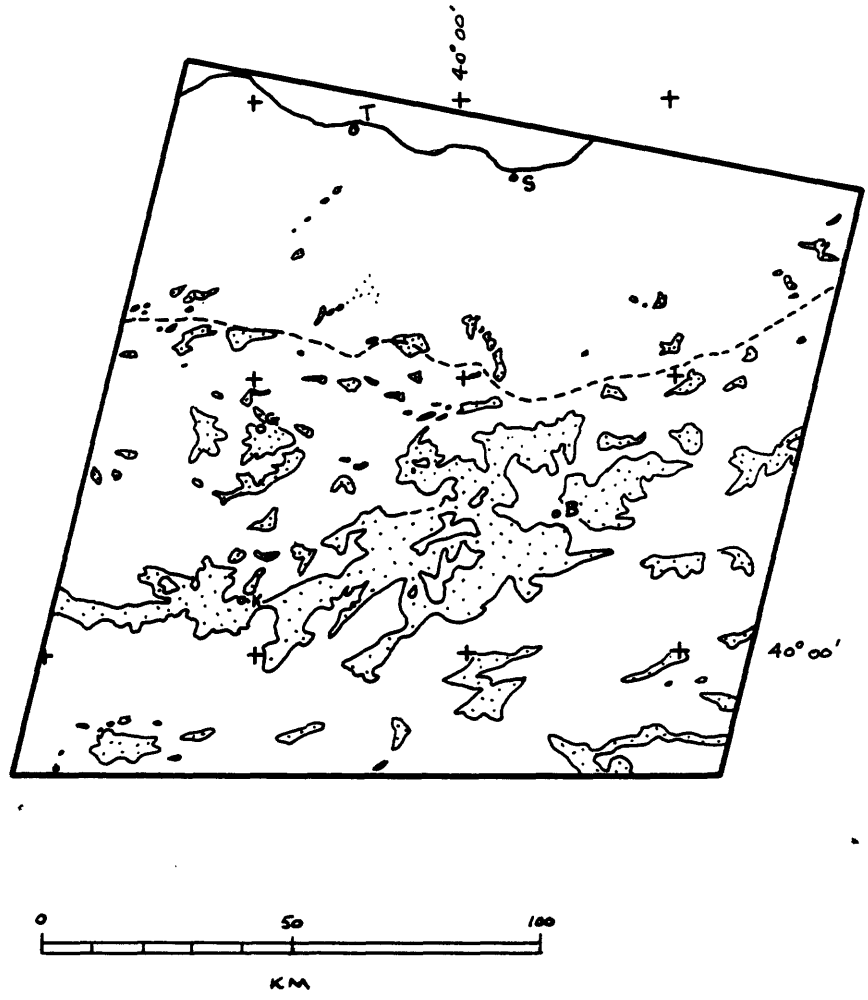

Figure 5. Map of limonitic areas (stippled pattern) derived from color-ratio-composite image. North of dashed line, and in topographically high areas south of line, limonite mapping incomplete because of dense vegetation cover.

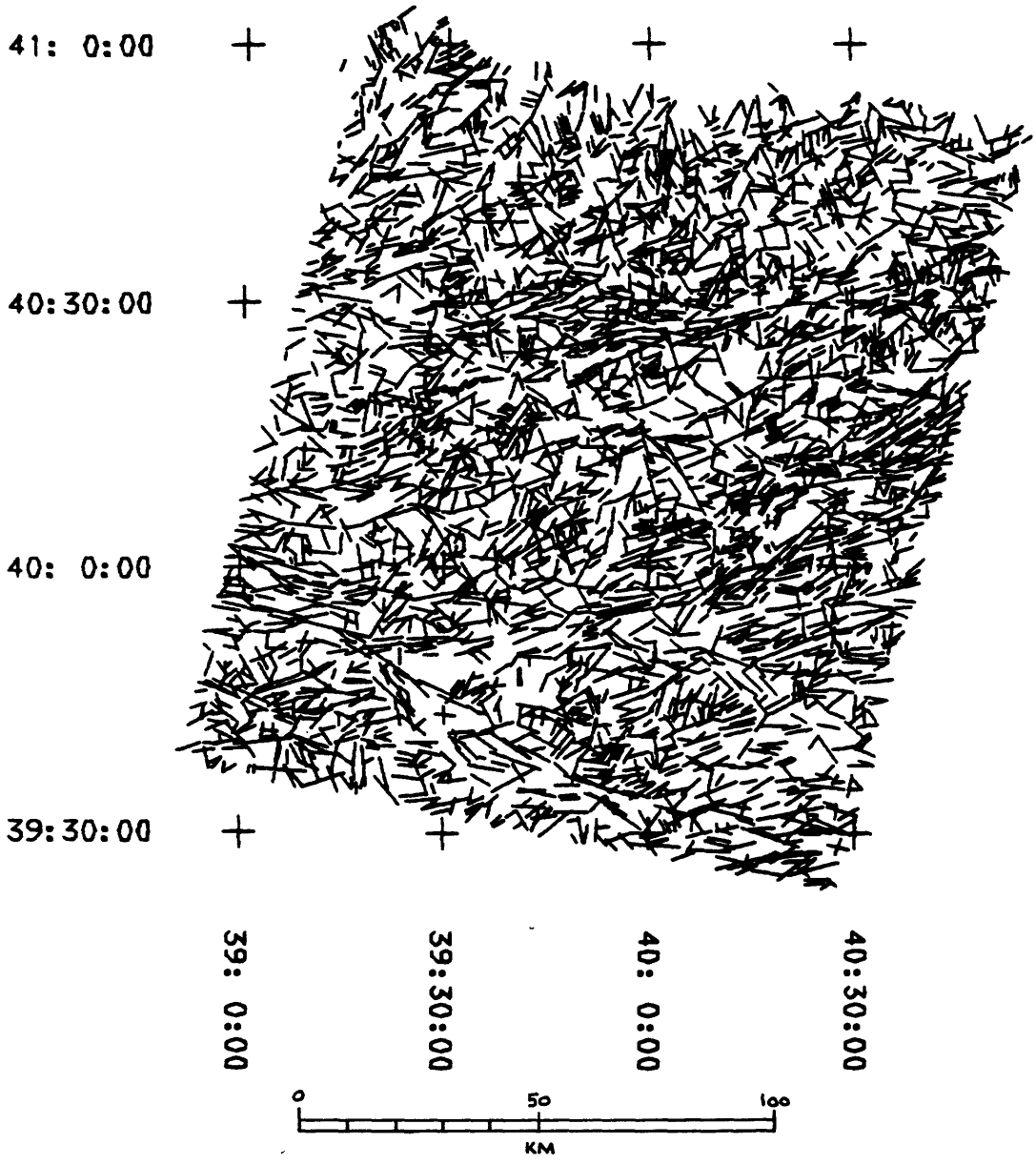

Figure 6. All LFs compiled from all sources. Scale of this map and following maps is about 1:1,500,000.

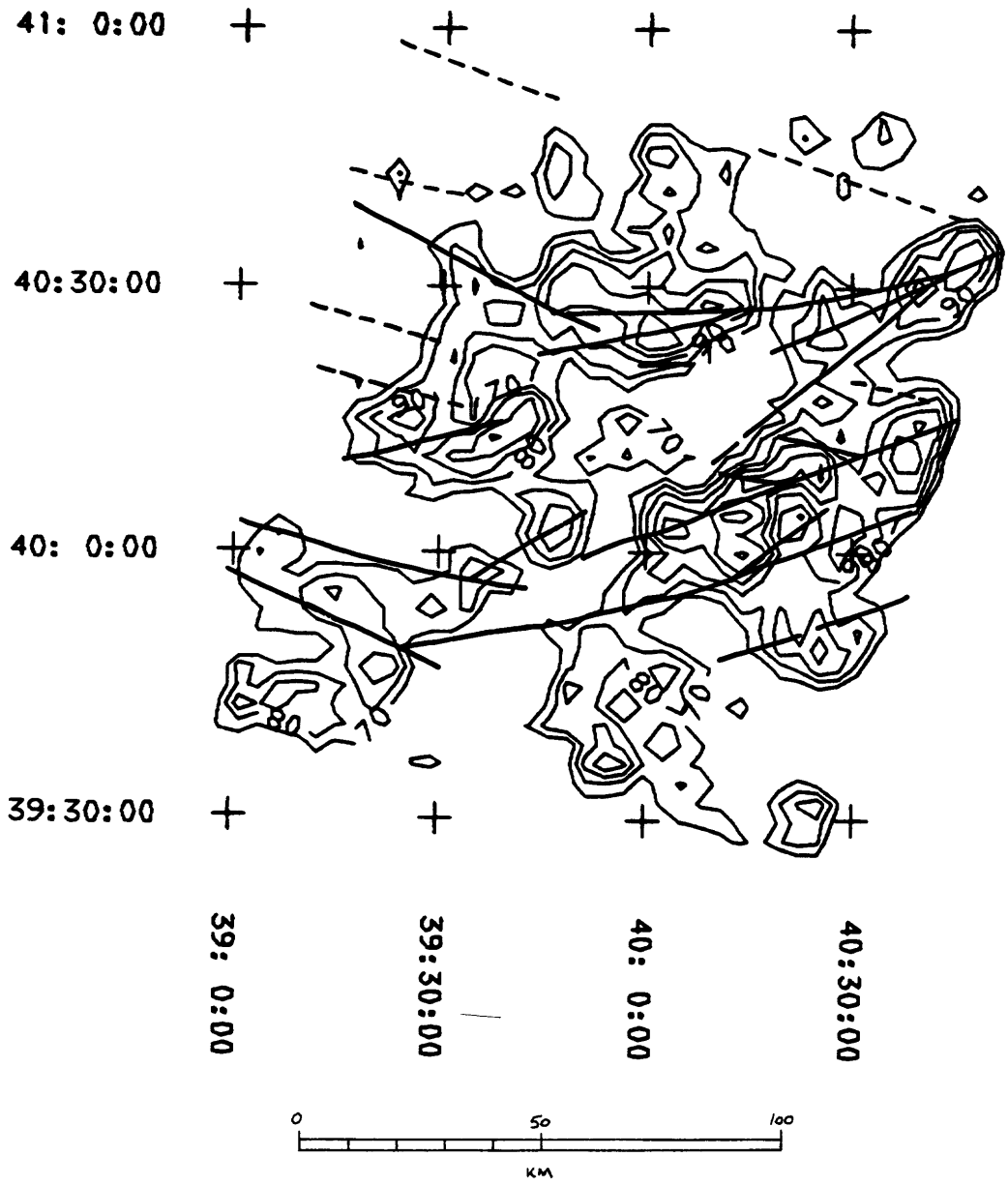

Figure 7. Concentrations of all linear features and derived lineaments. Contour values are relative numbers (southern part of map area was not of interest for uranium exploration; lineaments not continued south of latitude 39°50').

LENGTH INTERVAL		FREQUENCY	CUM FREQ	REL FREQ	+	+	+	+
0.00	0.40	0	0	0.00				
0.40	0.80	1	1	0.03				
0.80	1.20	13	14	0.39	*			
1.20	1.60	53	67	1.57	*****			
1.60	2.00	160	227	4.74	**********			
2.00	2.40	273	500	8.09	**********			
2.40	2.80	375	875	11.11	**********			
2.80	3.20	387	1262	11.46	**********			
3.20	3.60	349	1611	10.34	**********			
3.60	4.00	317	1928	9.39	**********			
4.00	4.40	287	2215	8.50	**********			
4.40	4.80	234	2449	6.93	**********			
4.80	5.20	167	2616	4.95	**********			
5.20	5.60	148	2764	4.38	**********			
5.60	6.00	101	2865	2.99	**********			
6.00	6.40	94	2959	2.78	**********			
6.40	6.80	83	3042	2.46	**********			
6.80	7.20	70	3112	2.07	**********			
7.20	7.60	55	3167	1.63	**********			
7.60	8.00	38	3205	1.13	**********			
8.00	8.40	25	3230	0.74	**********			
8.40	8.80	15	3245	0.44	**********			
8.80	9.20	15	3260	0.44	**********			
9.20	9.60	19	3279	0.56	**********			
9.60	10.00	9	3288	0.27				
0.00	10.40	17	3305	0.50	**********			
0.40	10.80	13	3318	0.39	**********			
0.80	11.20	16	3334	0.47	**********			
1.20	11.60	8	3342	0.24				
1.60	12.00	5	3347	0.15				
2.00	12.40	5	3352	0.15				
2.40	12.80	4	3356	0.12				
2.80	13.20	3	3359	0.09				
3.20	13.60	4	3363	0.12				
3.60	14.00	0	3363	0.00				
4.00	14.40	3	3366	0.09				
4.40	14.80	2	3368	0.06				
4.80	15.20	2	3370	0.06				
5.20	15.60	0	3370	0.00				
5.60	16.00	1	3371	0.03				
6.00	16.40	0	3371	0.00				
6.40	16.80	2	3373	0.06				
6.80	17.20	1	3374	0.03				
7.20	17.60	2	3376	0.06				

Figure 8. Histogram of lengths of all linear features, in kilometers. (cum freq = cumulative frequency; rel freq = relative frequency).

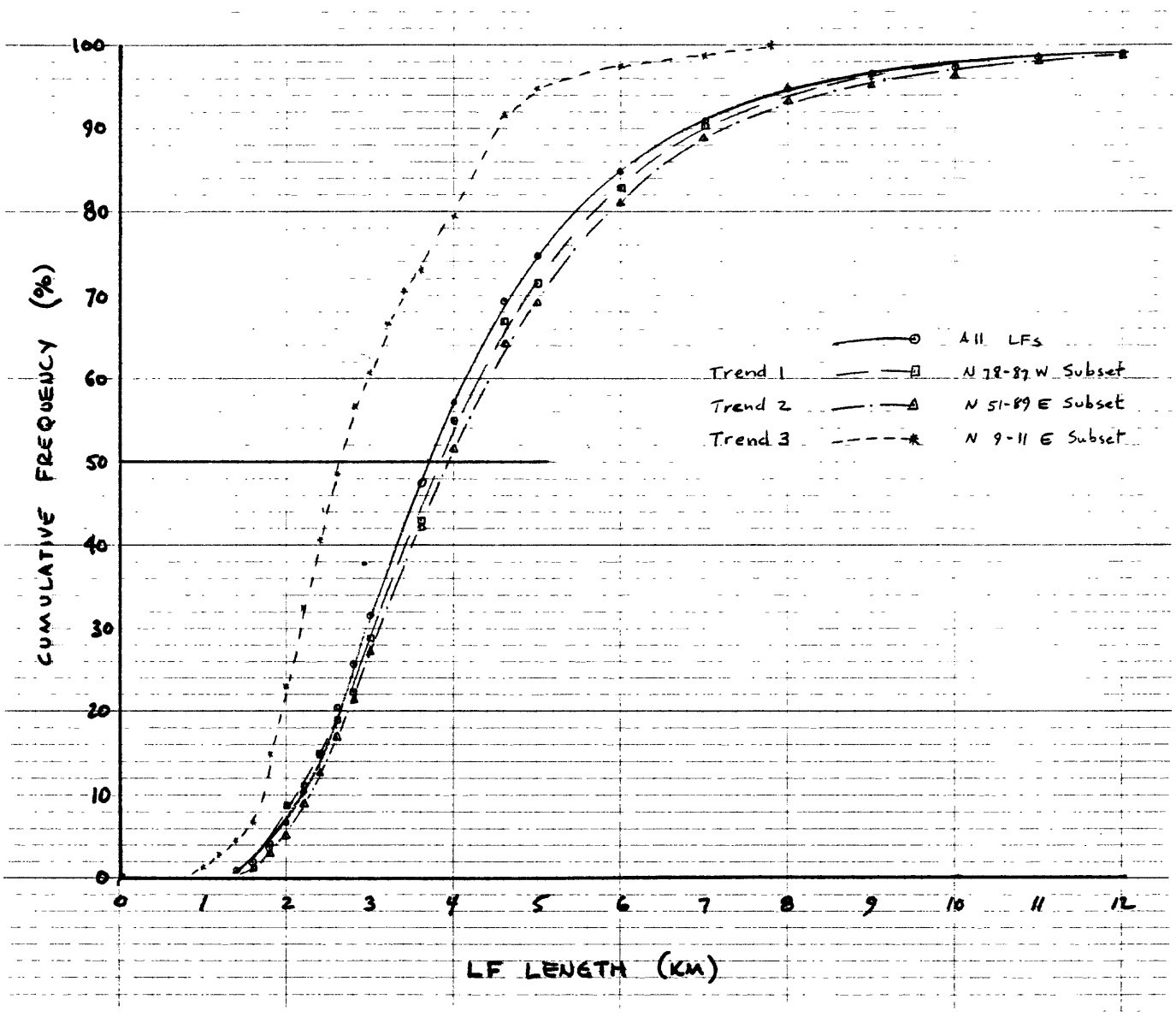

Figure 9. Cumulative frequency distributions of all linear features (LFs) and of selected trends.

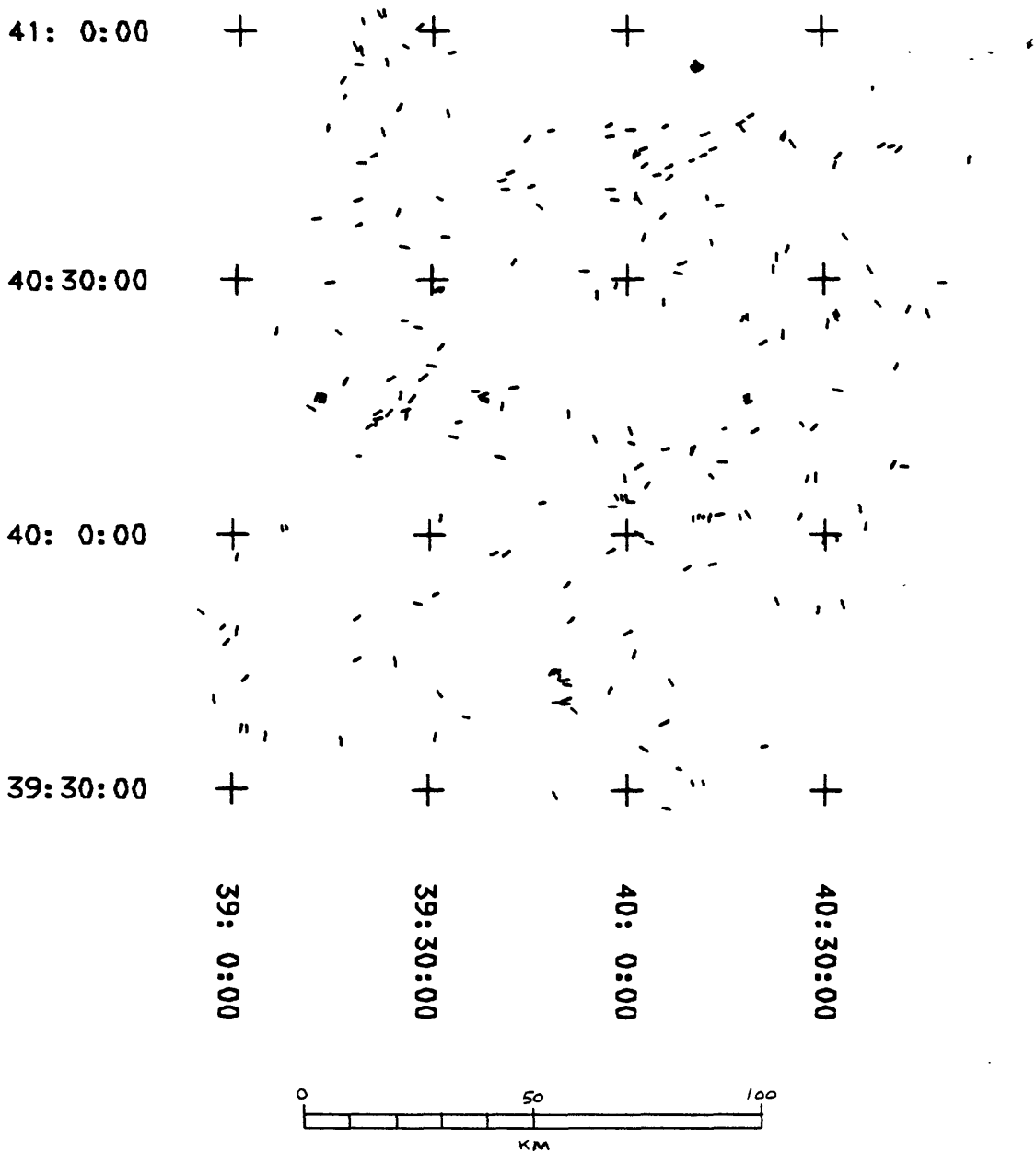

Figure 10. All linear features less than 2 km long.

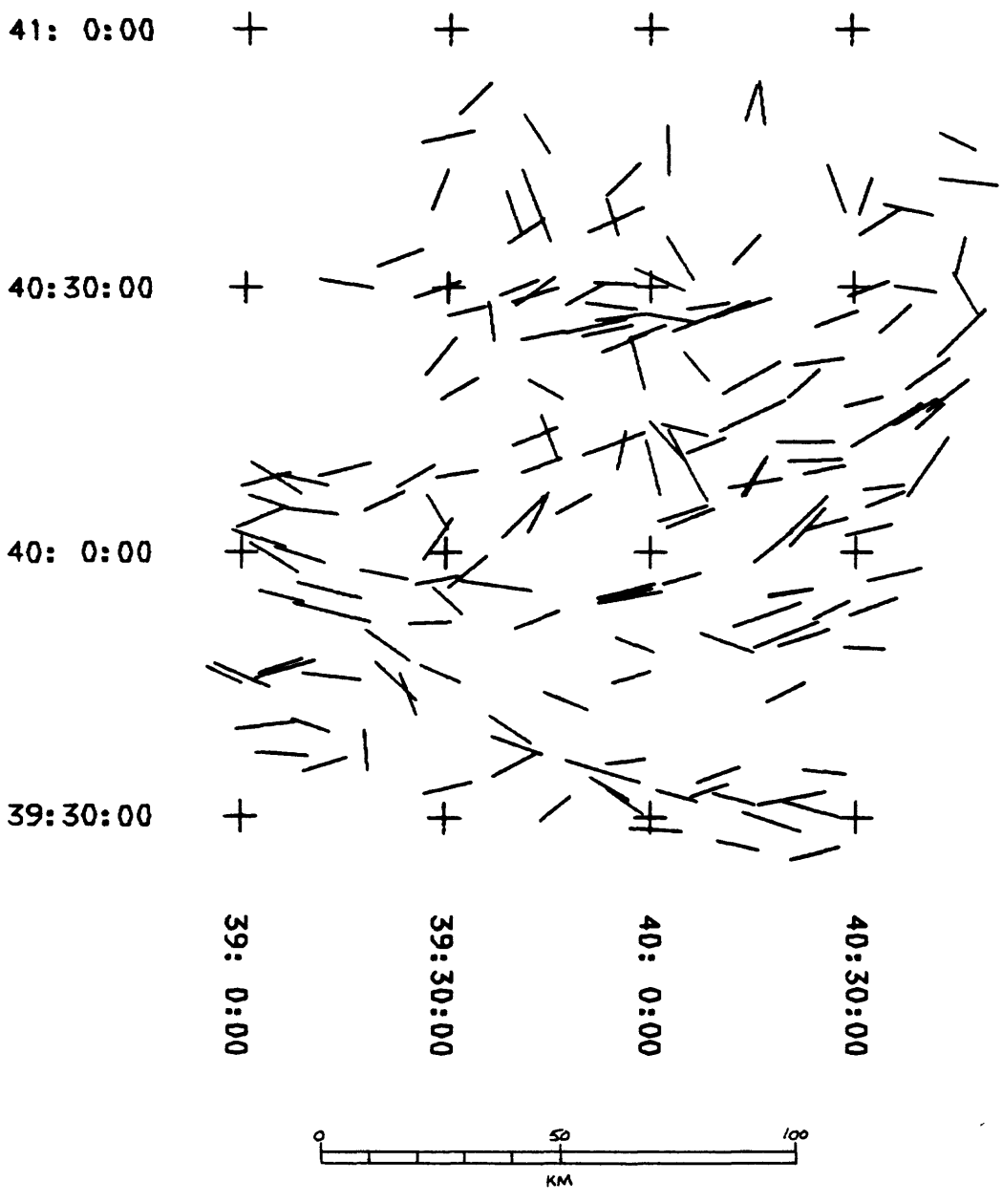

Figure 11. All linear features more than 8 km long.

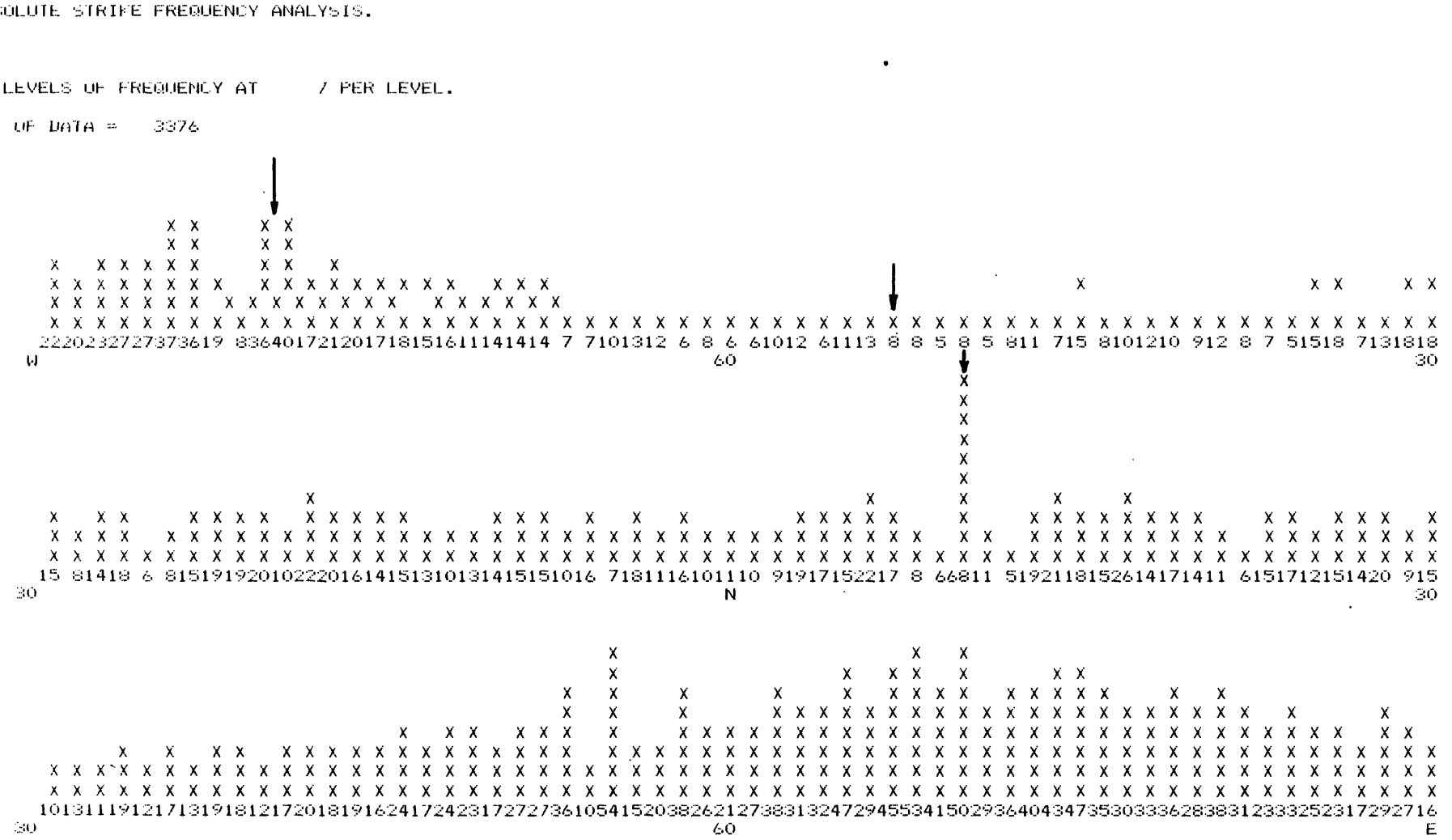

Figure 12. Strike-frequency distribution of all linear features. Arrows indicate orbit path (pixel edges) at N. 10° E., scanlines (pixel edges) at N. 80° W., and sun azimuth at N. 53° W.

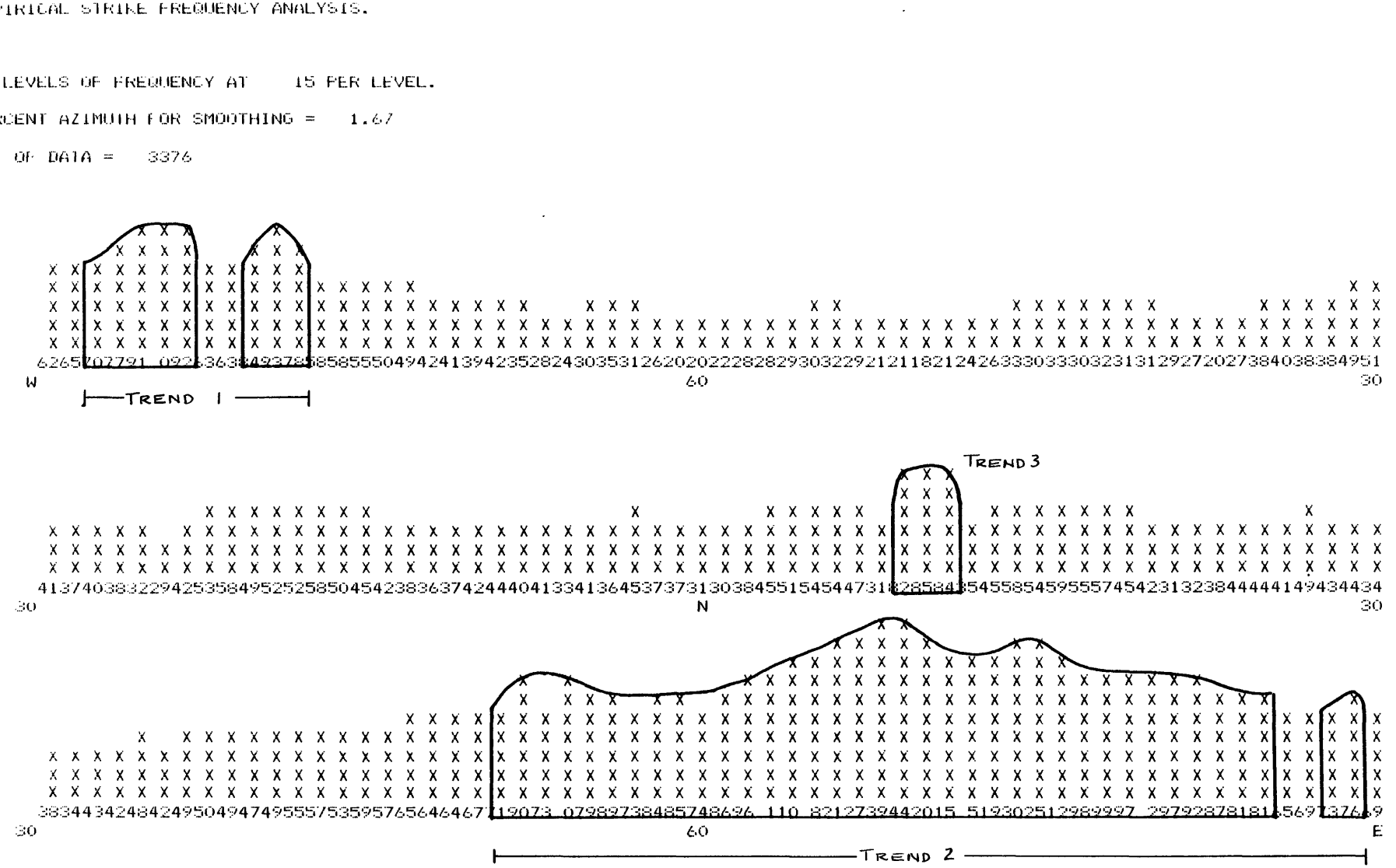

Figure 13. Smoothed strike-frequency distribution of all linear features. Trend intervals indicated where significance value greater than 90 percent.

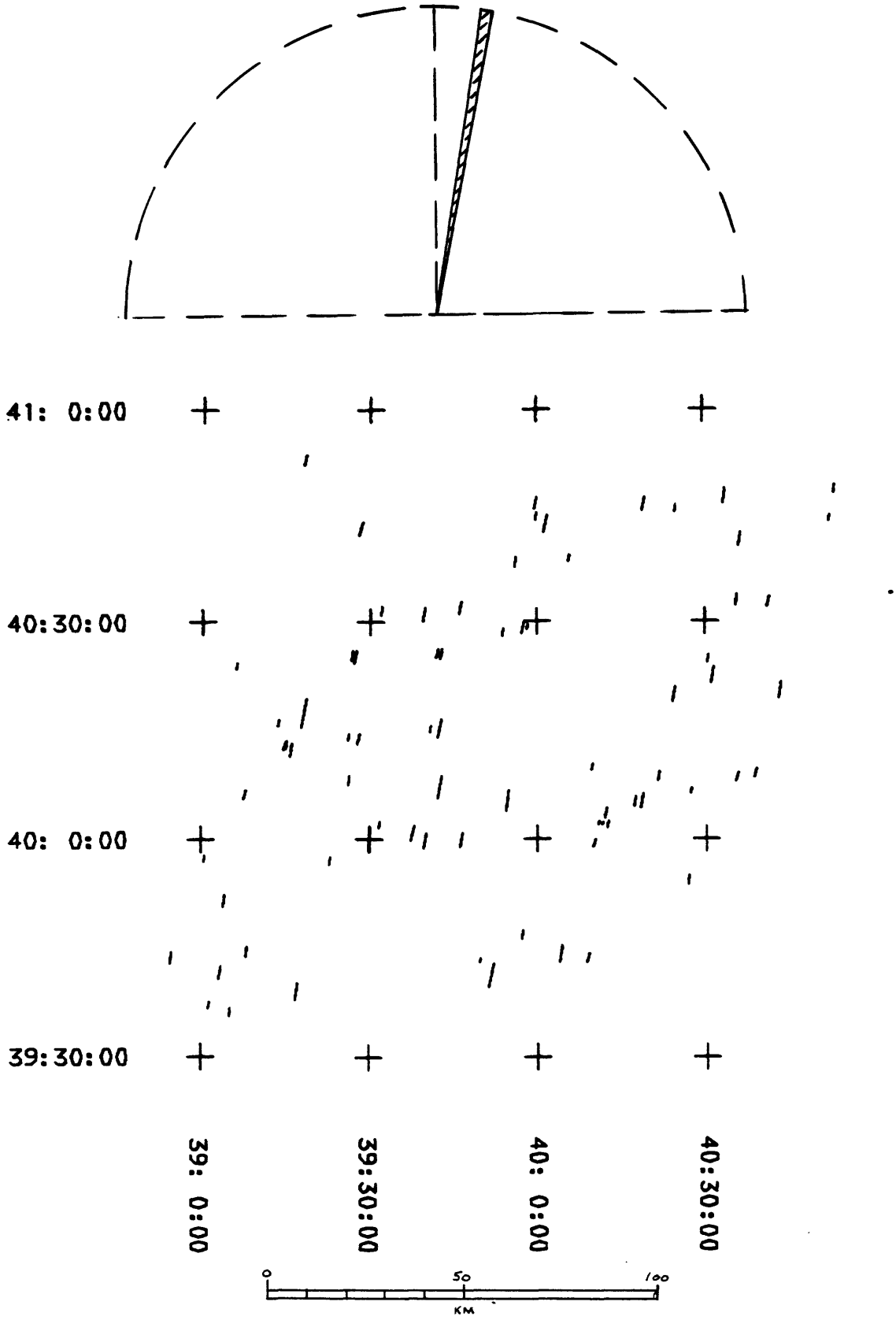

Figure 14. Subset of linear features with N. 9°-11° E. orientations (9-11).

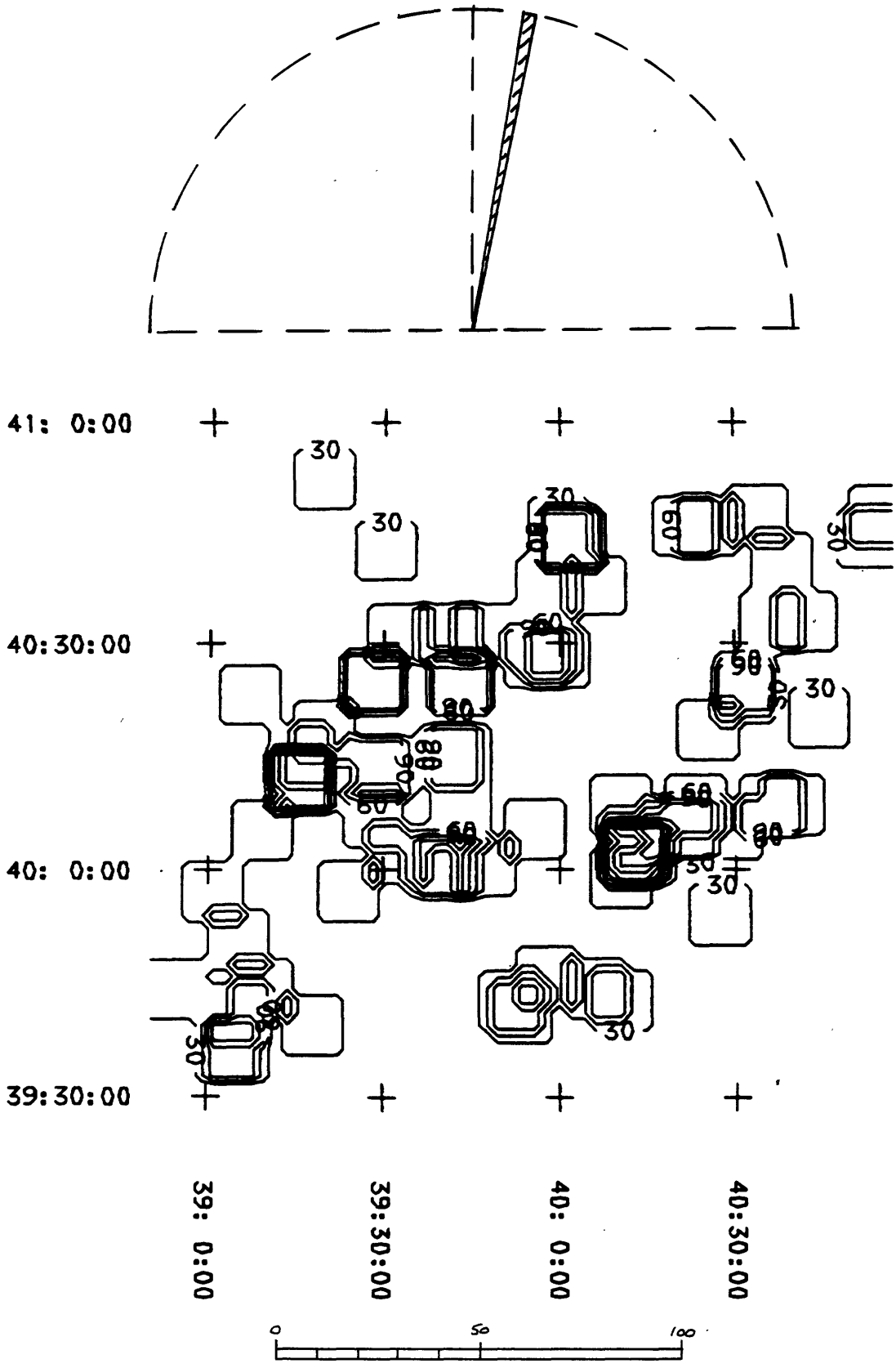

Figure 15. Concentrations of linear features with N. 9°-11° E. orientations (9-11).

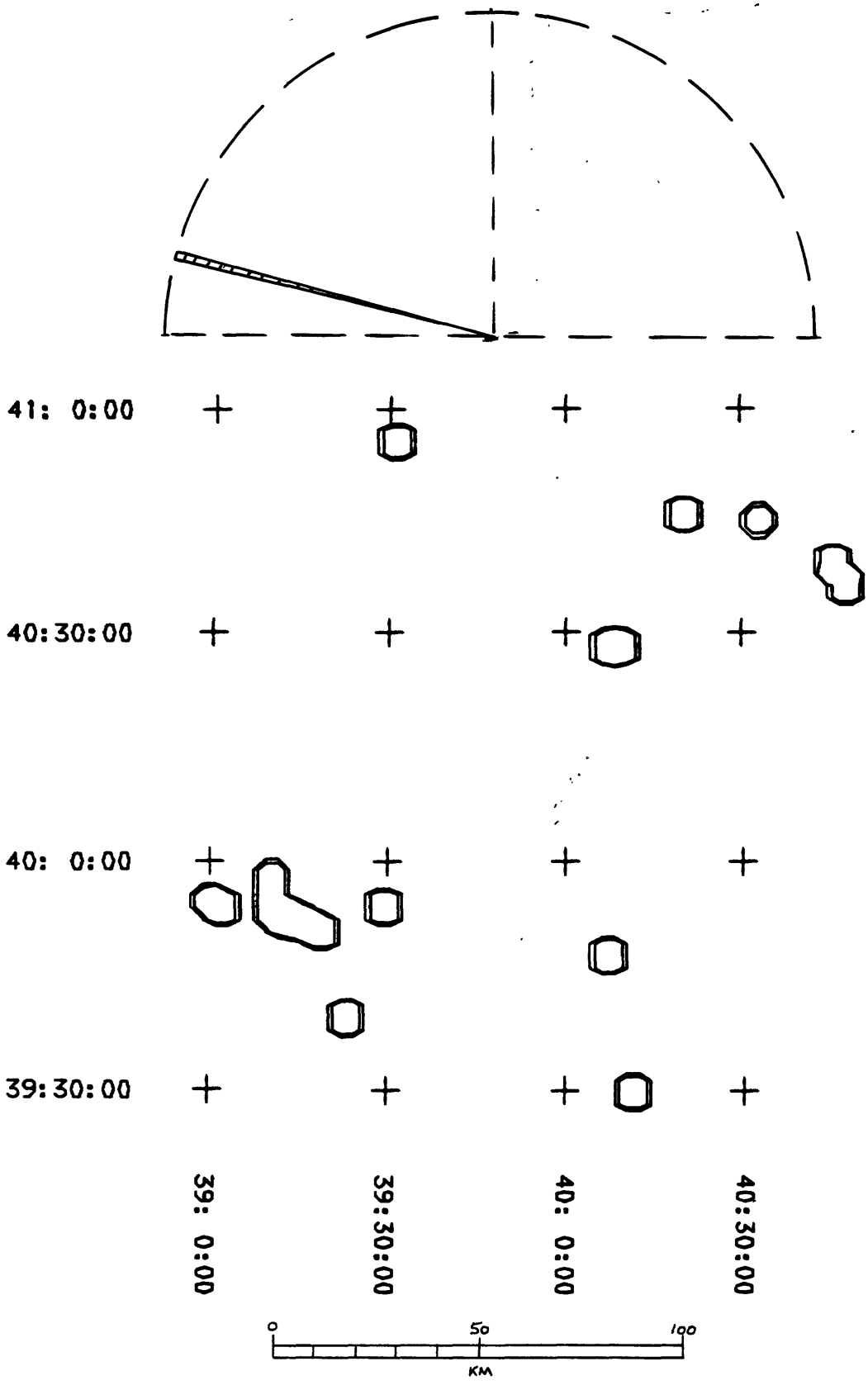

Figure 16. Concentrations of linear features with N. 75°-76° W. orientations (284-285).

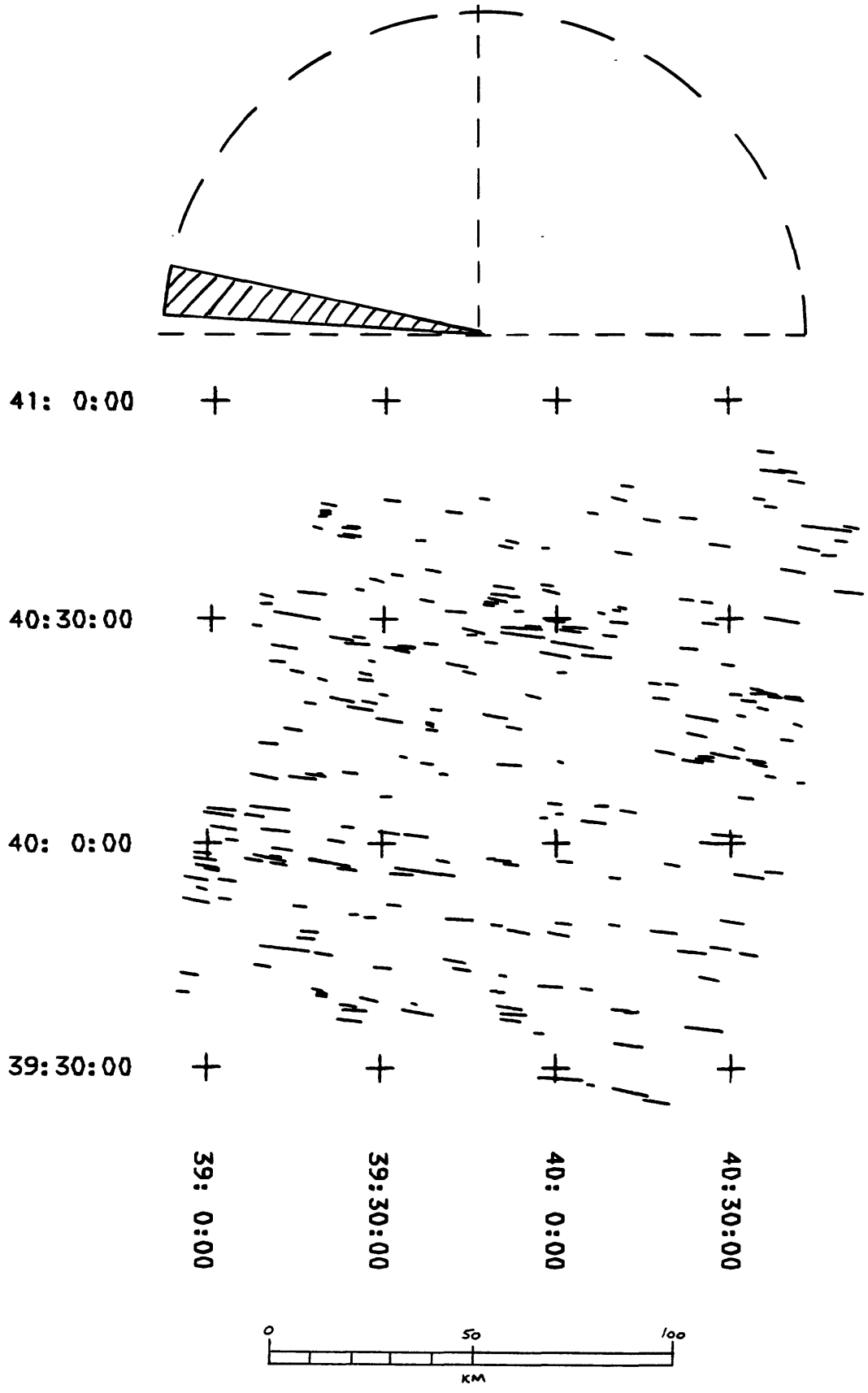

Figure 17. Map of Trend 1 linear features - N. 78°-87° W. (273-282).

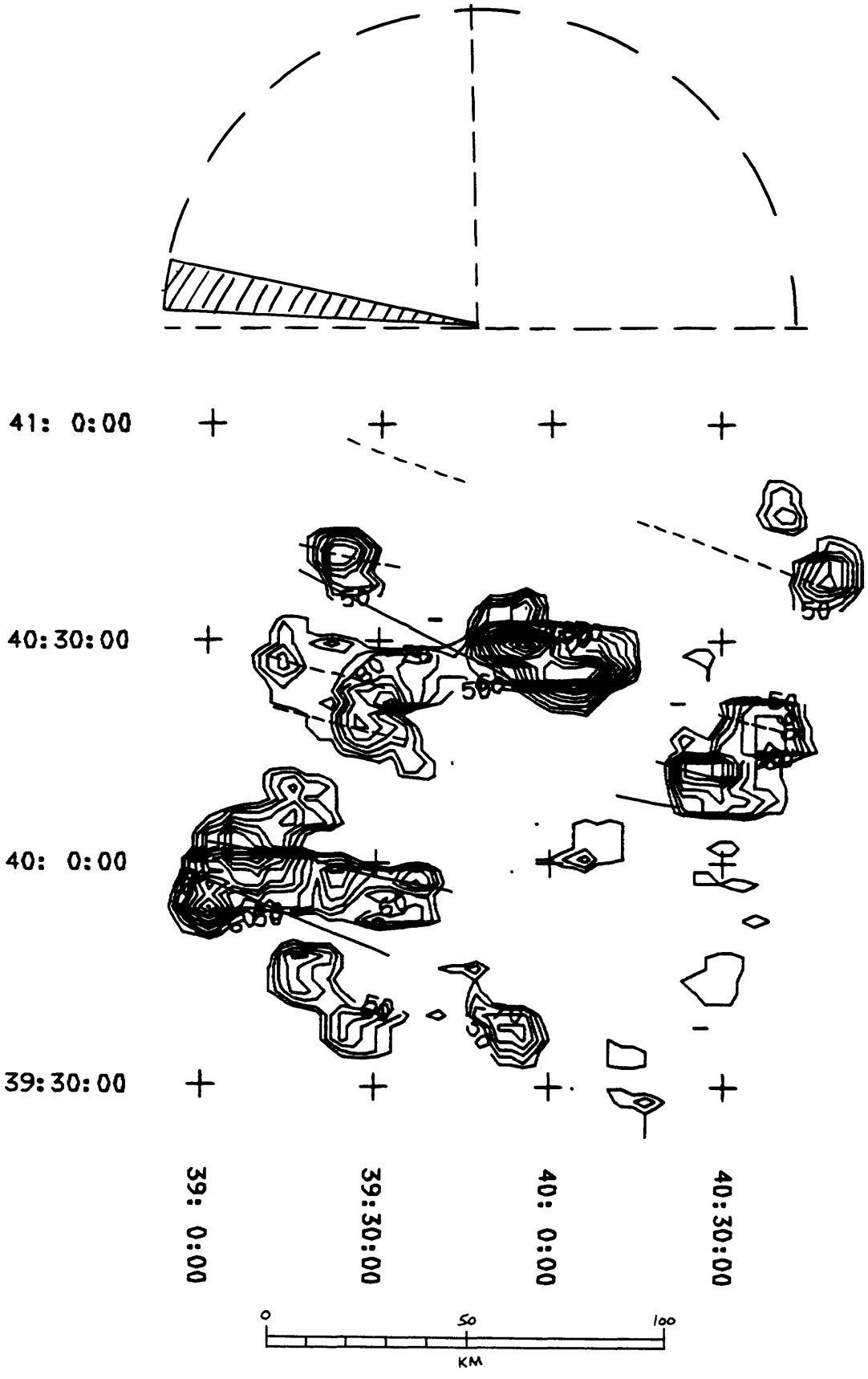

Figure 18. Concentrations of Trend 1 linear features - N. 78°-87° W. (273-282)- and derived lineaments (north of 39°50').

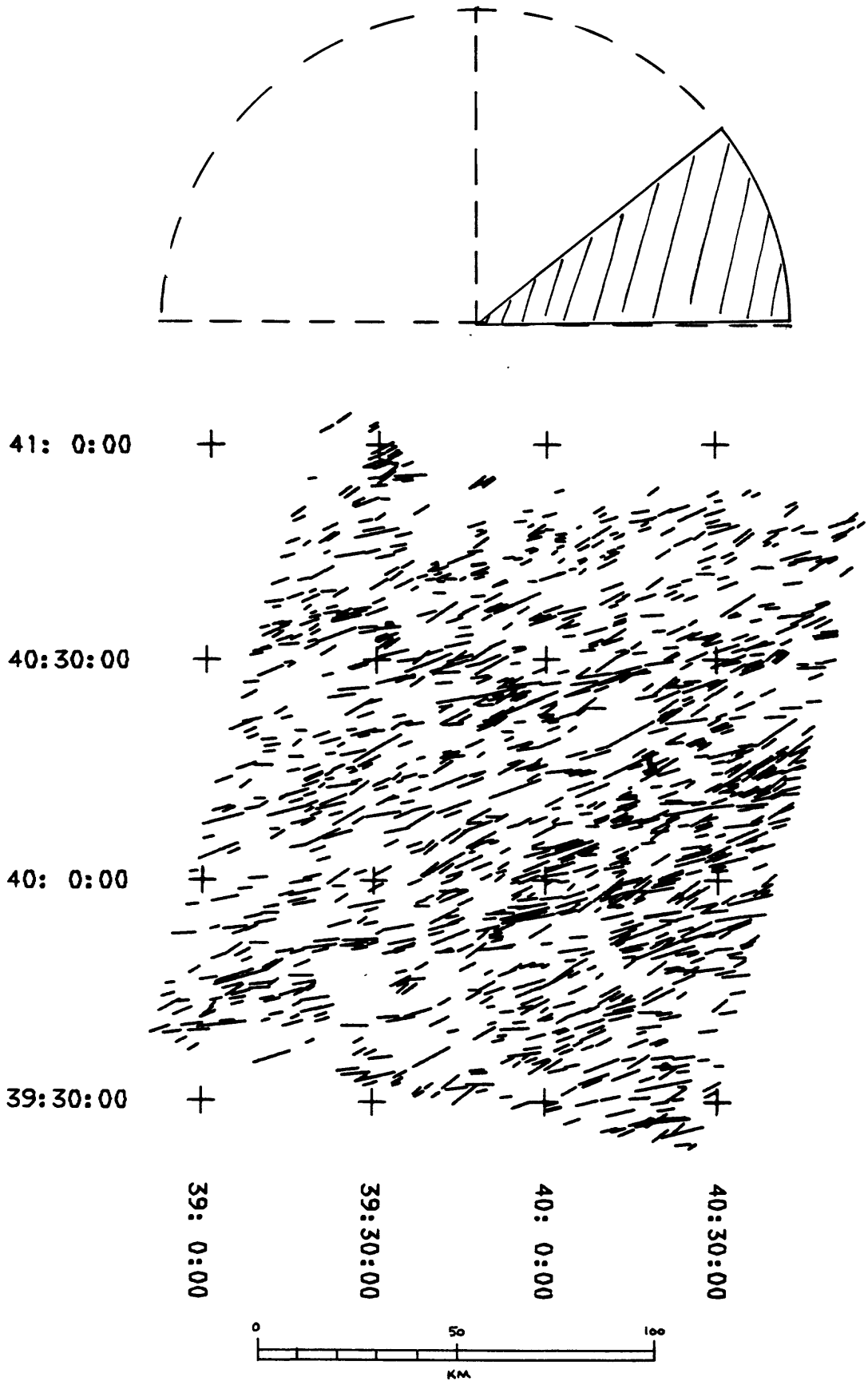

Figure 19. Map of Trend 2 linear features - N. 51°-89° E. (51-89).

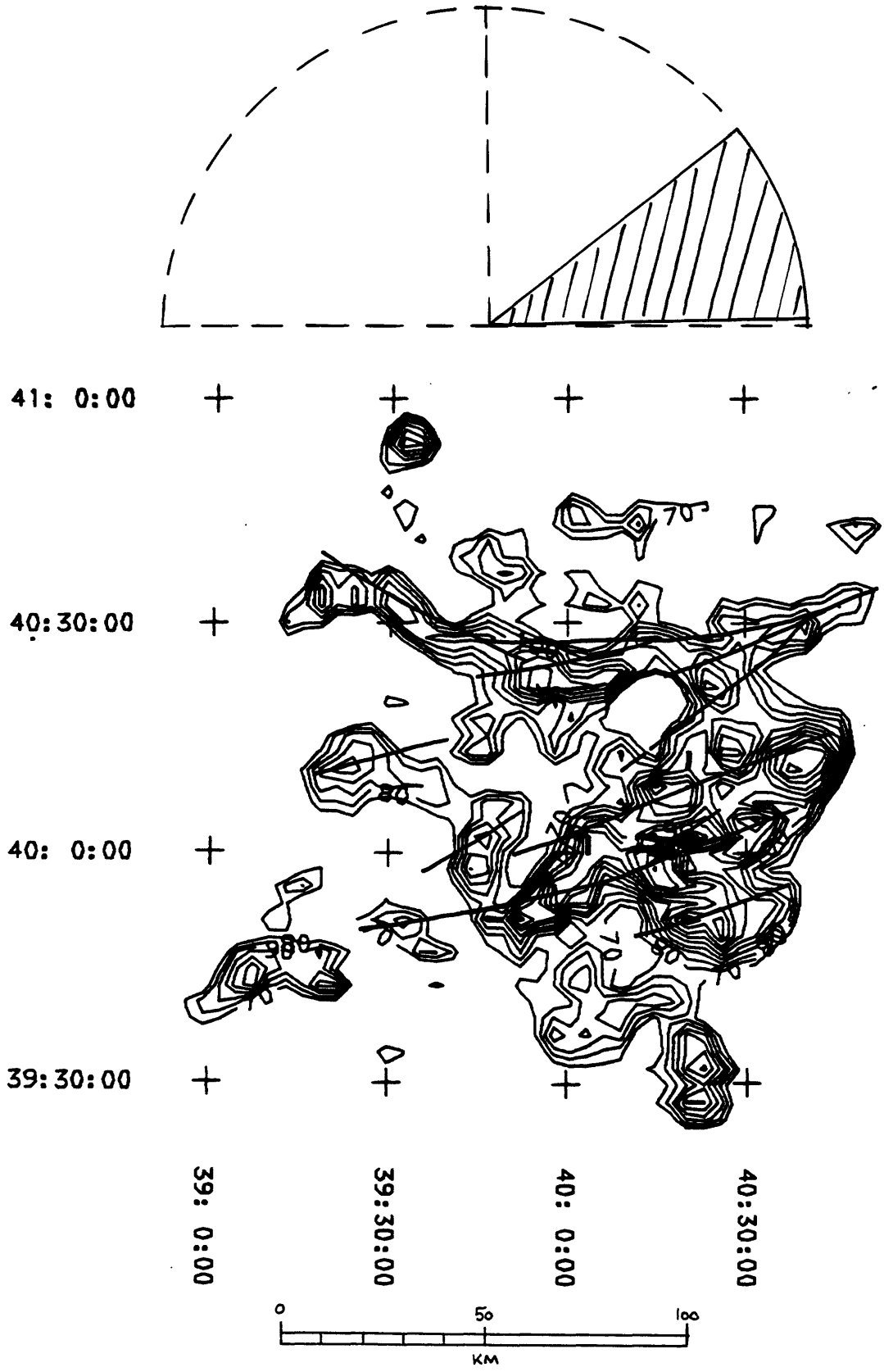

Figure 20. Concentrations of Trend 2 linear features - N. 51°-89° E. (51-89) - and derived lineaments (north of 39°50').

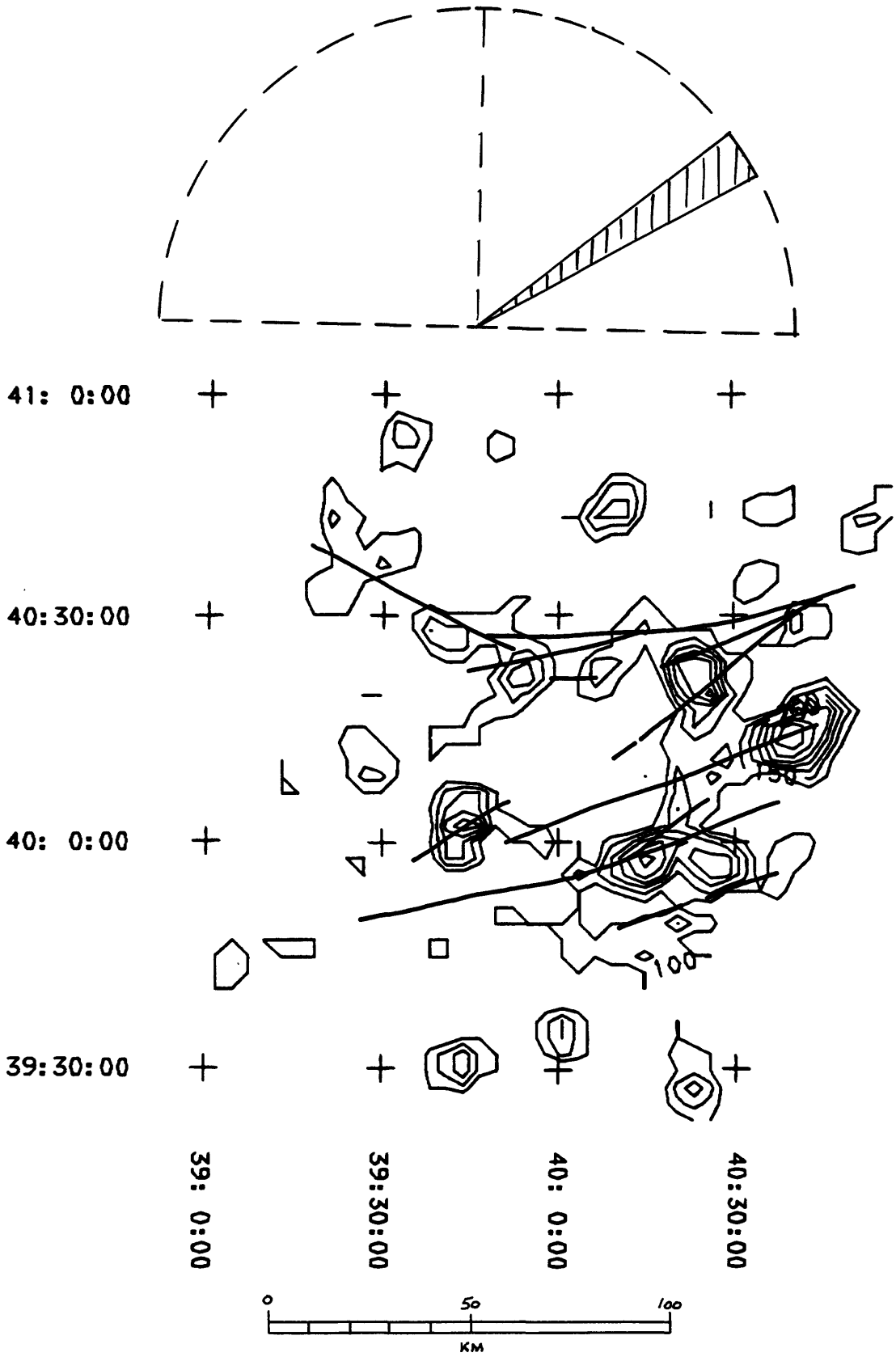

Figure 21. Concentrations of Trend 2 linear features - subset N. 51°-60° E. (51-60). Annotated lineaments include all of those lineaments derived from all of the Trend 2 linear features.

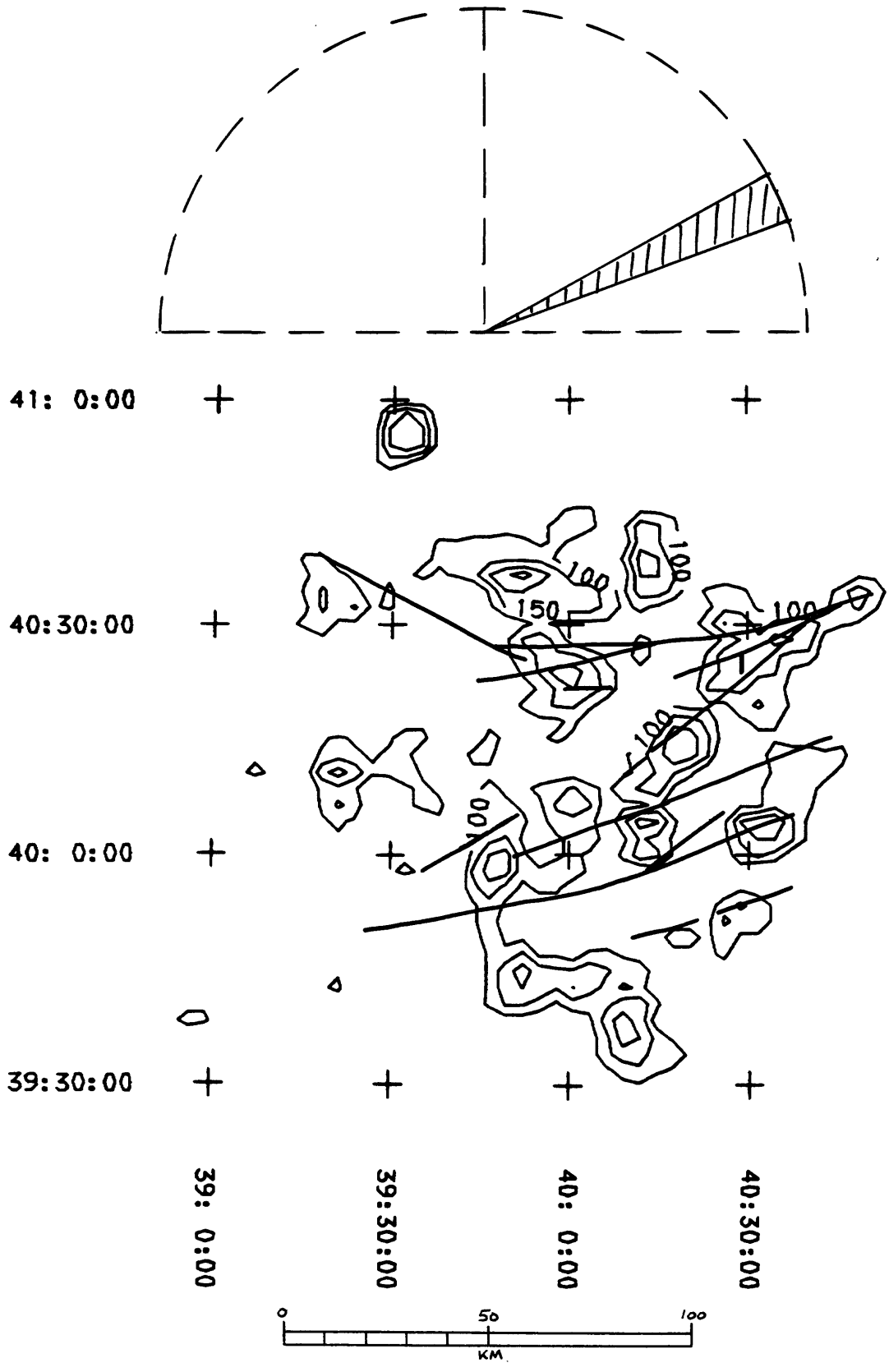

Figure 22. Concentrations of Trend 2 linear features - subset N. 61°-70° E. (61-70). Annotated lineaments include all of those lineaments derived from all Trend 2 linear features.

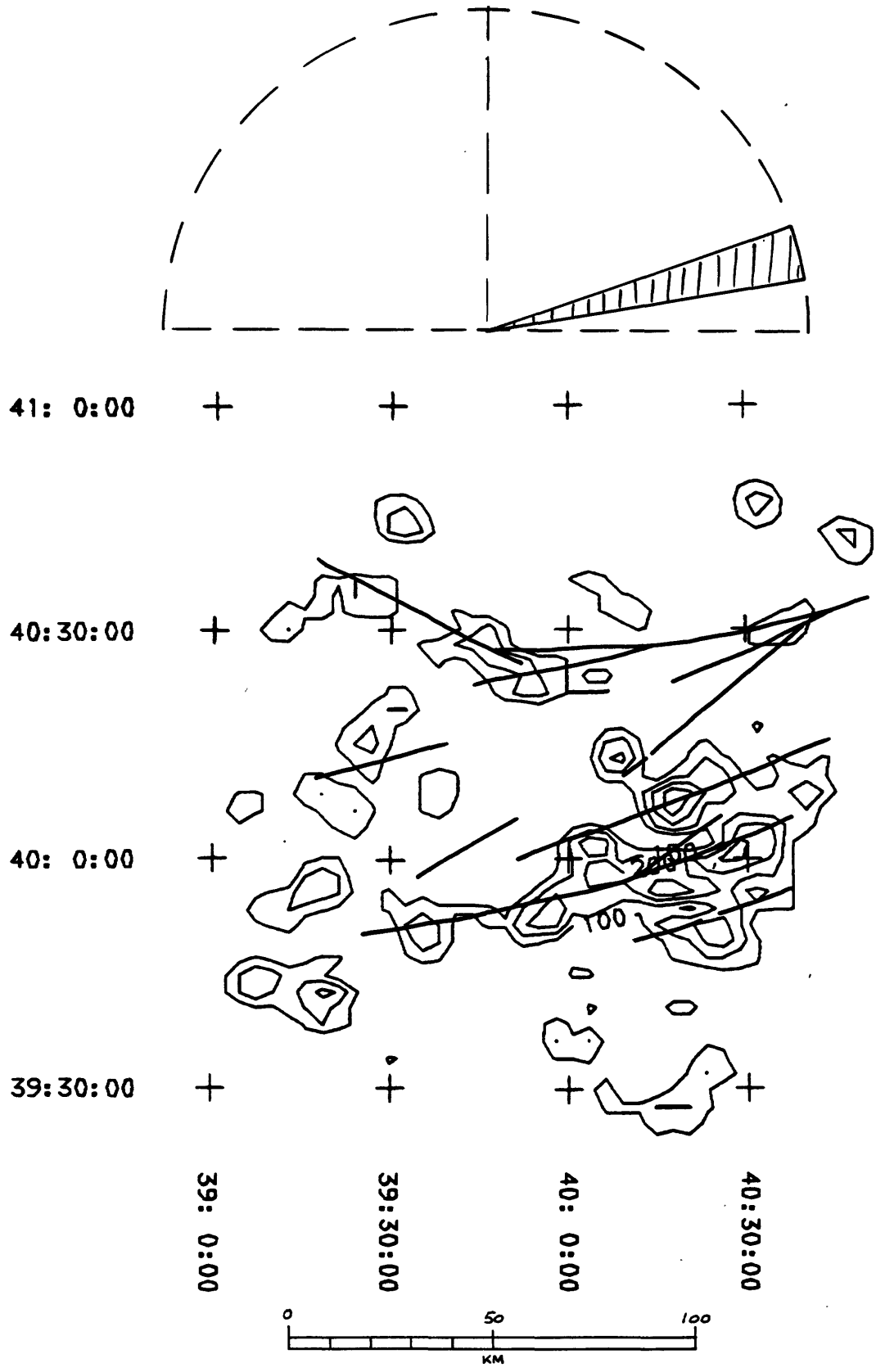

Figure 23. Concentrations of Trend 2 linear features - subset N. 71°-80° E. (71-80). Annotated lineaments include all of those lineaments derived from all Trend 2 linear features.

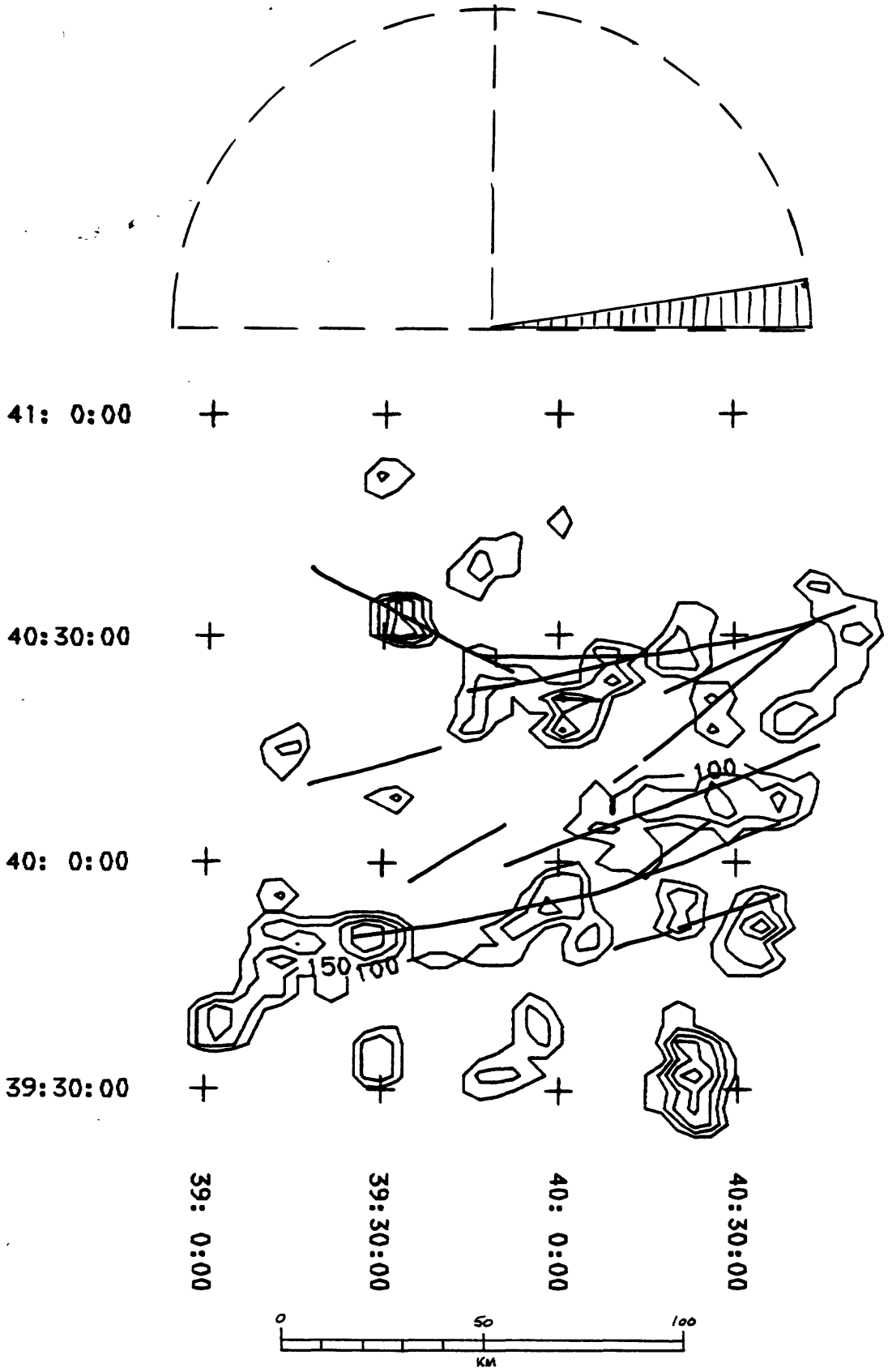

Figure 24. Concentrations of Trend 2 linear features - subset N. 81°-89° E. (81-89). Annotated lineaments include all of those lineaments derived from all Trend 2 linear features.

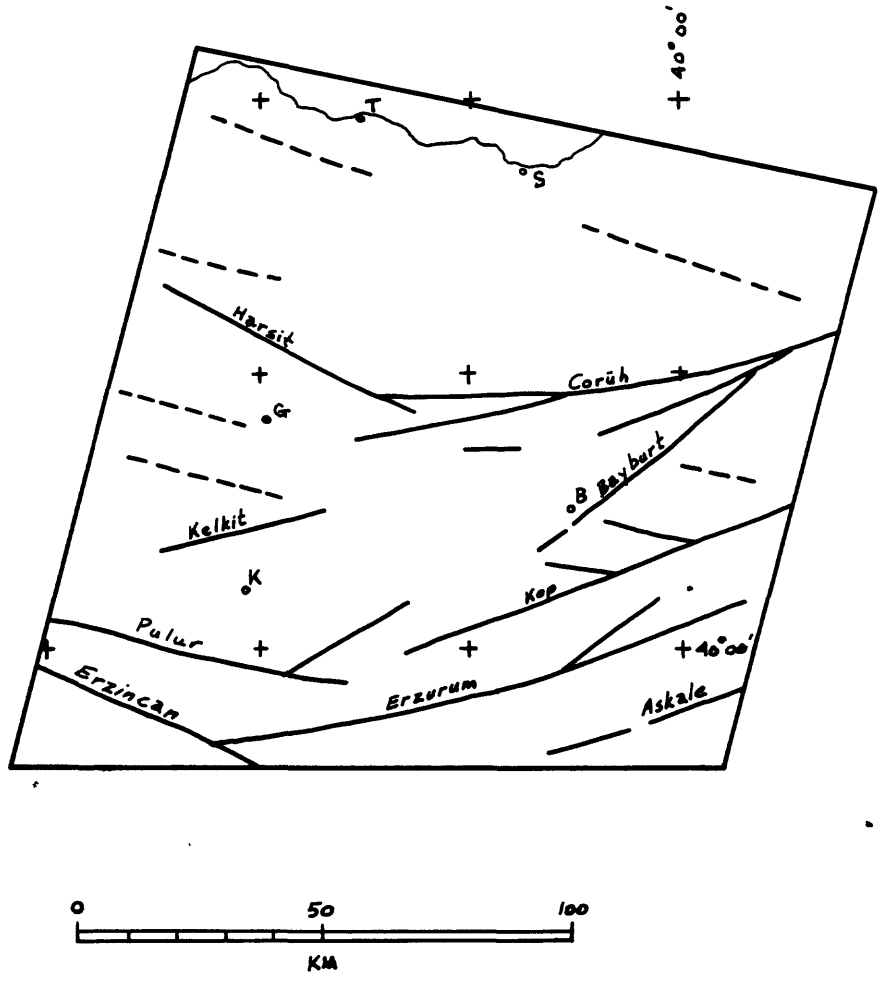

Figure 25. Lineaments derived from linear features analysis (dashed lines are weaker lineaments).

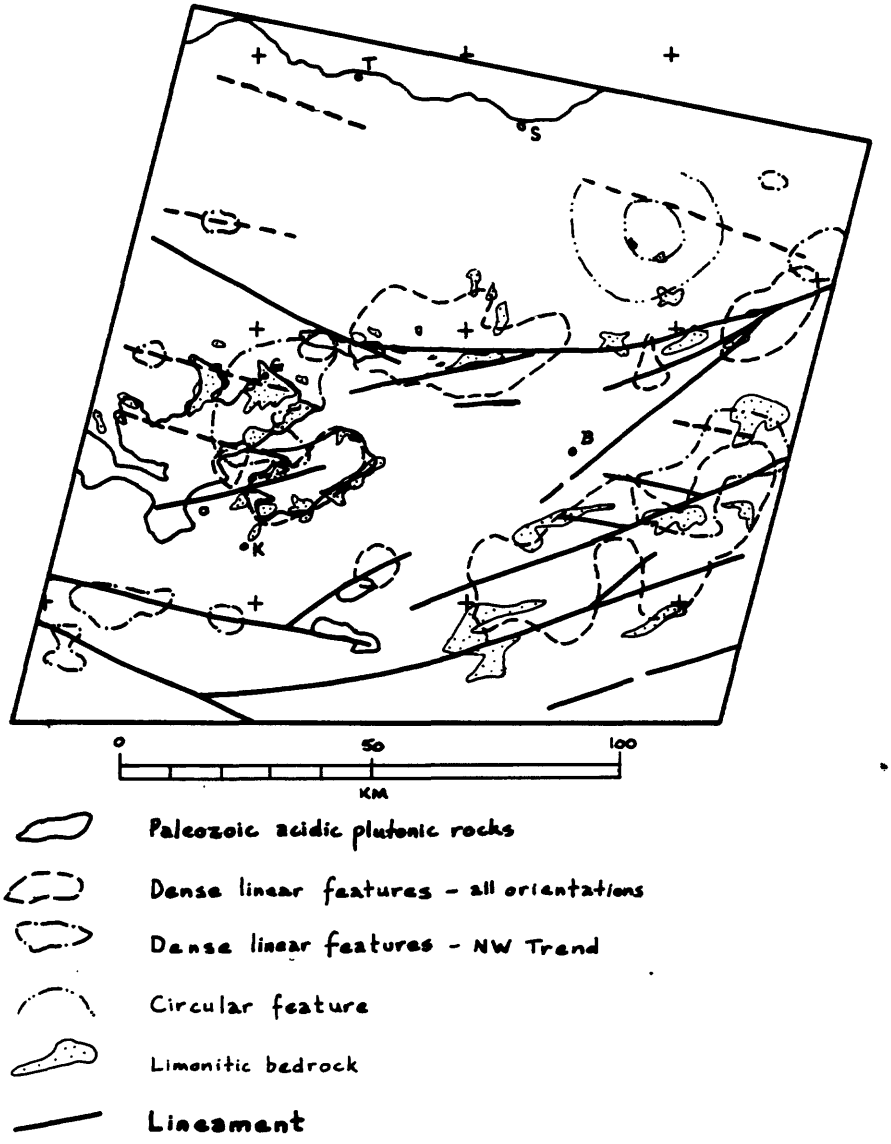

Figure 26. Exploration guides for uranium derived from Landsat images.